

To appear in The Astronomical Journal, January 2001

The Dwarf Galaxy Population of the Dorado group down to $M_V \approx -11$ ¹

Eleazar R. Carrasco and Cláudia M. de Oliveira

*Instituto Astronômico e Geofísico, Universidade de São Paulo
Caixa Postal 3386, 01060-970, São Paulo, Brazil*

rcarrasc@pushkin.iagusp.usp.br,oliveira@iagusp.usp.br

and

Leopoldo Infante^{2,3}

*Dep. de Astronomía y Astrofísica, Facultad de Física
Pontificia Universidad Católica de Chile, Casilla 306, Santiago 22, Chile*

linfante@astro.puc.cl

and

Michael Bolte

UCO/Lick Observatory, University of California, Santa Cruz, CA 95064

bolte@ucolick.org

ABSTRACT

We present V and I CCD photometry of suspected low-surface brightness dwarf galaxies detected in a survey covering $\sim 2.4 \text{ deg}^2$ around the central region of the Dorado group of galaxies. The low-surface brightness galaxies were chosen based on their sizes and magnitudes at the limiting isophote of $26.0V\mu$. The selected galaxies have magnitudes brighter than $V \approx 20$ ($M_V \approx -11$ for an assumed distance to the group of 17.2 Mpc), with central surface brightnesses $\mu_0 > 22.5 \text{ V mag/arcsec}^2$, scale lengths

¹Based on the data collected at the Cerro Tololo Interamerican Observatory and Las Campanas Observatory, Chile

²Visiting astronomer, Cerro Tololo Interamerican Observatory (CTIO). CTIO is operated by Association of Universities for Research in Astronomy Inc. (AURA), under a cooperative agreement with the National Science Foundation.

³Visiting astronomer, Las Campanas Observatory. Las Campanas is operated by the Carnegie Institution of Washington.

$h > 2''$, and diameters $\geq 14''$ at the limiting isophote. Using these criteria, we identified 69 dwarf galaxy candidates. Four of them are large very low-surface brightness galaxies that were detected on a smoothed image, after masking high surface brightness objects. Monte Carlo simulations performed to estimate completeness, photometric uncertainties and to evaluate our ability to detect extended low-surface brightness galaxies show that the completeness fraction is, on average, $> 80\%$ for dwarf galaxies with $-17 < M_V < -10.5$ and $22.5 < \mu_0 < 25.5$ V mag/arcsec², for the range of sizes considered by us ($D \geq 14''$). The $V - I$ colors of the dwarf candidates vary from -0.3 to 2.3 with a peak on $V - I = 0.98$, suggesting a range of different stellar populations in these galaxies. The projected surface density of the dwarf galaxies shows a concentration towards the group center similar in extent to that found around five X-ray groups and the elliptical galaxy NGC1132 studied by Mulchaey & Zabludoff (1999), suggesting that the dwarf galaxies in Dorado are probably physically associated with the overall potential well of the group.

Subject headings: galaxies: clusters: general – galaxies: photometry – galaxies: fundamental parameters (classification, colors, surface brightness) – galaxies: dwarfs: – galaxies: luminosity function – galaxies: cluster: individual (Dorado group)

1. Introduction

Dwarf galaxies are the most common type of galaxies in the local universe. In addition, they are thought to be the single systems with the largest dark-matter contents, with M/L ratios as high as that of groups and poor clusters (e.g. Carignan and Freeman 1988) and hence their spatial distribution and mass spectrum may give us important insights into the spatial scales over which mass is distributed. However, they are also the hardest galaxies to observe, due to their low-surface brightnesses and low luminosities. Only recently it has become possible to obtain deep wide-field CCD *photometry* of significant numbers of these galaxies, mostly in clusters. *Spectroscopy* of such low luminosity systems is still a challenge even with large-class telescopes, unless emission lines are present.

Dwarf galaxies in nearby clusters and groups have been studied in detail with photographic material (e.g. Coma: Thompsom & Gregory 1993; Virgo: Sandage, Binggeli and Tammann 1985, Impey et al. 1988; Fornax: Ferguson 1989; Bothun et al. 1991; groups: Ferguson and Sandage 1991). From these works two general trends were uncovered: 1) clusters and rich groups usually have a luminosity function with a faint end that is steeper, i.e., has more low-luminosity galaxies, than that for poorer groups and 2) Dwarf elliptical and dwarf spheroidal galaxies (dE/dS0) seem to dominate the faint-end of the number counts in clusters while the dwarf-irregular population (dIrr) are more representative in poor groups and in the field. Point (1) was well illustrated by Ferguson & Sandage (1991) who found a faint-end slope (fit to a Schechter function) of $\alpha = -1.3$ in

the composite luminosity function of seven nearby groups (the sample included the Dorado group) with a tendency for the richer groups to present a larger ratio of dwarf to giant galaxies than the poorer groups. Point (2) has been challenged by observations of the most well known group of all, our own Local Group. Despite being a poor group with just over 30 members, the Local Group has a larger number of dE/dS0 than of dIrr (Pritchet & van den Bergh 1999). The majority of the dwarf spheroidal galaxies are concentrated around M31 and the Milky Way with a slope of the faint-end of the luminosity function (fit to a Schechter function) of ~ -1.3 while the dwarf irregulars are less concentrated with a flat luminosity distribution (van den Bergh 1999, Grebel 2000). This seems to contradict the results obtained for the CfA groups and field survey where the largest contribution to the steep faint-end was from the irregular galaxies (Marzke et al. 1998). Recent results coming from CCD studies in nearby groups up to $D = 10$ Mpc show an increasing number of new dwarf members (e.g. Jerjen et al. 2000) with a spatial distribution similar to that found in the Local Group (i.e the dwarf spheroidals concentrated around the brightest galaxies while the irregulars distributed throughout the group).

This is the first paper of a series dedicated to survey nearby groups with the aim of identifying low-surface brightness dwarf galaxies (hereafter LSBG) down to $M_V \sim -11$. Our primary goal is to study the physical properties and luminosity distributions of the LSBG and ultimately determine the luminosity function of the groups as a function of their richness and other group parameters. Here we report the results of the CCD photometry of the dwarf galaxy candidates of the nearby group of galaxies Dorado. A further study will analyze other nearby groups of galaxies.

The Dorado group is a loose concentration of galaxies centered at $\sim 4^h 15^m, -55^\circ 41'$ (epoch J2000). It is also known as Shk 18 (Shakhbazian 1957), G16 (de Vaucouleurs 1975) and HG3 (Huchra & Geller 1982). Dorado was first identified by de Vaucouleurs (1975) as a “large and complex nebulae” in the region of Dorado. In 1982, Huchra & Geller (1982), measured velocities for 18 galaxies in the group. Maia et al. (1989) extended the number of known members to 46. Finally Ferguson & Sandage (1990, 1991), in a study of the galaxy properties in seven nearby groups identified 34 possible members of Dorado with magnitudes $B_T > 19$ in photographic plates. The central part of the group is dominated by two almost equally bright early-type systems: NGC1549 (an E1 galaxy with $V_r = 1247$ km/s) and NGC1553 (an S0 galaxy with $V_r = 1280$ km/s). No detailed distance determination has been made for Dorado and therefore we will adopt a group distance of $17.2 h^{-1}$ Mpc, where $h = H_0/75$. This was determined for the central galaxy NGC1549 based on the D_n - σ relation from Faber et al. (1989). For the determination of the absolute magnitudes of the galaxies we chose the value of $H_0 = 75$ km s $^{-1}$ Mpc $^{-1}$. The group covers an area on the sky of $\sim 10^\circ \times 10^\circ (\sim 3 \times 3 h^{-1}$ Mpc).

This paper is arranged as follows. Section 2 describes the observations, the data reduction and the methodology used to detect, classify and to obtain photometric parameters for galaxies in the frames. In that section we also describe the Monte-Carlo simulations performed in order to estimate the completeness for the LSBG population, and to determine the distribution of detected central surface brightness and scale lengths to be expected if Local Group and Virgo-like LSBG

were present in the Dorado group. In section 3 we present the results and analyze the central surface brightness, scale length, spatial and color distributions of the LSBD candidates. Finally, in section 4, a general discussion and a brief summary of the main results are presented. The luminosity function of the group will be determined, along with those for other groups, in a later publication.

2. Observations and data reduction

2.1. Observations

The Dorado group was observed in two separate runs at the end of 1996. The central region of the group was observed on November 1–2, with the 0.9m Curtis/Schmidt telescope at the Cerro Tololo Interamerican Observatory (hereafter CTIO). The images were obtained using a standard STIS 2048 × 2048 pixel CCD with 21 μm pixels corresponding to 2.028''/pixel on the sky. The total field of view was 1°15 × 1°15. The second set of observations was performed with the 1.0m Swope telescope at the Las Campanas Observatory (hereafter LCO40), Chile, in the nights of December 2-7, 1996. In this case the Tektronix 5 CCD, with 2048 × 2048 21- μm pixels (0''696 on the sky) was used. The total field of view per image was 24' × 24'.

The fields were imaged through standard Johnson *V* and Cousins *I* filters. Typical total exposure times were between 30 and 60 min per field in both filters. All data were taken under photometric conditions, with a seeing ranging from 1''3 to 1''9 in the LCO40 frames. Due to the large pixel size of the CCD used in the observations taken at CTIO (2.028''/pix), the image quality in the central field is much worse than that for the LCO40 images ($\sim 3''$). Table 1 shows the observation log (field identification, equatorial coordinates, filters, observatories, exposure times, the observed area and the area used on the analysis after the masked pixels were disregarded) where D01 is the central field observed in CTIO and D02 to D11 are the fields observed in LCO40. The total area covered by the observations was $\sim 2^\circ 6$ ($\sim 1^\circ 2$ in the central region and $\sim 1^\circ 4$ spread over the outskirts of the group) in each of the filters. After subtraction and masking the bright objects in the fields, the total area used in the analysis was $\sim 2^\circ 4$. Figure 1 shows the sizes and locations of the observed CCD images. The symbols indicate the galaxies with known velocities taken from the NED. In addition, we observed two fields 10° north (B3) and 15° south (B4) of the Fornax galaxy NGC 1399, in order to estimate the background contamination of low surface brightness galaxies. These observations were performed in the second run (LCO40), with the same filters and exposure times matching the Dorado LCO40 observations (see Table 1 for details).

2.2. Reductions and photometric calibrations

The images were bias/overscan-subtracted and trimmed, using the CCDPROC task inside IRAF¹. Dome and twilight flats were combined with the object-frames taken during the night to make a master flat-field and used to flat-field the data. The images were then combined by obtaining their median. The final combined images had an average *rms* pixel-to-pixel variation of the sky level that corresponded to a limiting surface brightness of ~ 26.2 (CTIO) and ~ 26.8 V mag/arcsec² (LCO40) for the V filter and ~ 25.2 (CTIO) and ~ 26 (LCO40) for the I filter. In the case of the LCO40 I frames, there were small scale variations along the CCD and since these could affect the analysis of the structural parameters of the LSBD, we decided to do the photometry on the I images using the V images as templates (i.e. using the same positions, ellipticities and areas obtained for objects in the V filter). The main use of the I photometry was to determine aperture colors for the objects.

Calibrations of the magnitudes to the standard system were derived using observations of standard stars from Landolt (1992). A number of standard stars were observed throughout the nights for that purpose: 26 and 22 during the two nights for CTIO and 42, 46, 47, 47 and 44 in the five nights for LCO40. The task APPHOT in IRAF was used to determine the instrumental magnitudes of the stars. Transformation equations from the instrumental to the standard Johnson-Kron-Cousins system were obtained using the following relation:

$$\begin{aligned}
 V &= v + a_0^v + a_1^v X_V + a_2^v (V - I) \\
 I &= i + a_0^i + a_1^i X_I + a_2^i (V - I) \\
 (V - I) &= \frac{[(v + a_0^v) - (i + a_0^i)] + a_1^i X_I - a_1^v X_V}{1 - (a_2^v - a_2^i)}
 \end{aligned}
 \tag{1}$$

where v and i are the instrumental aperture magnitudes of the standard stars, a_0^v and a_0^i are the transformation coefficients between the standard and instrumental system, a_1^v and a_1^i are the extinction coefficients, and a_2^v and a_2^i represent the coefficients of the color term. The calibration equations and coefficients for both CTIO and LCO40 runs are given in Table 2 (col. 4). The *rms* of the difference between standard and calibrated magnitudes for the standard stars is less than 0.025 mag (col. 5 in Table 2). We can see in Table 2 that the color coefficients are small and stable during the nights (LCO40 observations). The zero point for each filter was obtained using the two first equations of (1) and the coefficients given in Table 2 with an assumed color index of $(V - I) = 1$, a typical value for the LSBD population in nearby groups and clusters like Virgo (Impey & Bothun 1997). Magnitudes and colors were then calibrated accordingly.

¹IRAF is distributed by NOAO, which is operated by the Association of Universities for Research in Astronomy Inc., under contract with the National Science Foundation

2.3. Detection and photometry of the objects

Detection, photometry and classification of objects were performed using the Source Extractor (SExtractor) software program (Bertin & Arnouts 1996). Before running SExtractor, we removed all bright galaxies and saturated stars. These are necessary steps since otherwise the bright objects may have either prevented detection of faint sources or significantly affected the photometry of objects located in their wings. Figure 2 shows the central region of the Dorado group observed at CTIO (upper panel) with some examples of low surface brightness dwarf galaxies detected in this region (see below). The four brightest galaxies in the field, NGC1549, NGC1553, NGC1546 and IC2058 are marked on the figure (upper panel). These four galaxies were extracted from the frames, first by fitting their isophotes using the task STSDAS.ISOPHOTES.ELLIPSE. Then, their fitted ellipses were subtracted from the frame using the task BMODEL. Objects which were poor fits to elliptical isophotes were simply masked. Masking was also used to remove bright saturated stars and the remaining residuals from the bright elliptical galaxies subtraction. The same procedures were applied to subtract or mask the bright galaxies and stars from the LCO40 frames. In these frames only one galaxy was subtracted using the fitting technique (NGC1536 in D05). These pixels, corresponding to the masked areas, were not used in subsequent analysis.

The analysis of the image with SExtractor proceeded as follow: *i*) in each CCD image the background map was constructed using sub-areas of 64×64 pixels ($\sim 130 \times 130$ arcsec) and 128×128 pixels ($\sim 90 \times 90$ arcsec) for CTIO and LCO40 images respectively. These values are much larger than the typical size of a low-surface brightness galaxy that could be detected at the distance of the group (searches for larger galaxies were conducted in Section 2.7); *ii*) the local background histogram was clipped iteratively until convergence at 3σ was reached. These raw background values were filtered using a median filter (in 3×3 sub-areas), and a bi-cubic-spline was used to obtain the resulting background map. This background map was then subtracted from the image; *iii*) the images were convolved with a *top-hat* mask with a FWHM slightly larger than the values for the stellar images, in order to enhance the efficiency in detecting low-surface brightness, extended objects. All objects with a threshold ≥ 26 V mag/arcsec² ($\sim 1.2\sigma_{sky}$ and $\sim 1.7\sigma_{sky}$ for the CTIO and LCO40 frames respectively) above the sky level and with a minimum area of 5 pix² were found and their photometric parameters obtained (note that a threshold of $\sim 1.2\sigma_{sky}$ for the LCO40 images correspond to a limiting surface brightness of ~ 26.6 V mag/arcsec², i.e. 0.6 V mag/arcsec² fainter than our limiting surface brightness). We used a threshold of 26 V mag/arcsec² in order to have a common surface brightness cut in both the CTIO and the LCO40 fields.

Photometry of all objects in the *V* and *I* frames was done using elliptical apertures. Total magnitudes were computed using the Kron’s “first moment” algorithm $r_1 = \sum rI(r)/\sum I(r)$ (Kron 1980, Infante 1987). For each object, the elliptical apertures are chosen and the ellipticity and the position angle are defined by the second-order moments of the light distribution. The maximum aperture is then defined as one that has double the area of the isophotal elliptical aperture. Inside this aperture, the integrated light is used to construct a growth curve where the first moment is

computed. As discussed by Infante (1987) and Infante & Pritchett (1992), the $2r_1$ measures about 90% of the flux for galaxies with exponential profiles, and about 96% for objects with stellar profiles. We checked these values with Monte Carlo simulations (see section 2.6). It may also underestimate the true total magnitude for galaxies with $r^{1/4}$ intensity profiles, as suggested by Secker & Harris (1997). However, the number of faint group galaxies with $r^{1/4}$ is small.

The object detection was performed in the V filter and was used as a template to obtain the photometric parameters in the I filter (i.e. we forced the detection in the I filter of those objects detected in the V filter using common structural parameters). The output catalogues in both filters were then matched in order to obtain color information for all objects. Colors were determined by measuring magnitudes in a circular aperture of $7''$ of diameter in the CTIO field and $4''$ in the LCO40 fields, in both filters. Those objects centered within $\sim 10''$ of any edge or masked region in the images were deleted from the catalogues. The output matched catalogues (available under request) contain the isophotal magnitude, the isophotal area, the total magnitude, the ellipticity, eight isophotal areas which correspond to different surface brightnesses (see section 2.5), the peak surface brightness in mag/arcsec^2 (this corresponds to the intensity at the central pixel), coordinates at epoch J2000.0, a quality flag and the star/galaxy classification for each object.

The completeness of our sample for point sources falls below 90% at magnitudes $V \sim 20.5$ mag and $V \sim 23$ mag for the CTIO and LCO40 observations respectively (see section 2.6). For the I fields, the completeness falls to 90% at magnitudes $I \sim 19$ mag and $I \sim 21$ mag for the CTIO and LCO40 observations respectively.

2.4. Star/Galaxy separation

The star/galaxy separation (resolved = galaxies, unresolved = stars, globular clusters, unresolved background galaxies) was done with a neural network routine developed by Bertin & Arnouts (1996). This is a training program that classifies objects with an index (stellarity index) between 0 (galaxies) and 1 (stars). It uses eight isophotal areas (see section 2.5), the peak intensity, and the seeing to classify the objects. The star/galaxy separation works well down to $V \sim 20$ (CTIO) and $V \sim 22$ (LCO40). Objects with magnitudes beyond this limit present an increasing scatter in the classification.

In order to check the star/galaxy classification given by SExtractor we first did a visual inspection of all objects classified as galaxies with “stellarity index” less or equal than 0.3. The choice of 0.3 is based on our Monte Carlo simulations (section 2.6) since galaxies that mimic Local Group LSBG at the distance of Dorado are classified in all cases with stellarity indices lower than 0.3. Eye control showed that the classification of galaxies is adequate down to $V \sim 20.0$ and $V \sim 22.0$ for the CTIO and LCO40 respectively. For fainter magnitudes, the classification is uncertain. An alternative method was used to check the classification. This method consisted in plotting pairs of parameters like the central intensity *vs.* area, the central intensity *vs.* size of the objects, and

the peak intensity *vs.* size of the objects. For each plot, a curve was drawn in order to define the boundaries between stars and galaxies. Then, the classifications obtained from each of the three plots were combined to assign to each object a probability that it is a star, a galaxy or noise. We found that $\gtrsim 92\%$ of the galaxies were classified identically by this method, by SExtractor (“stilarity index” ≤ 0.3) and by the visual inspection down to $V \sim 20$ and $V \sim 22$ mag for the CTIO and the LCO40 frames respectively. The remaining objects were difficult to classify and these were labeled with an “uncertain” flag.

2.5. Selection of the low-surface brightness dwarf galaxy candidates

Selection of the LSBD candidates was done using parameters given by the exponential profile fit (the central surface brightness and scale length), and the diameter at the limiting isophote. Below we describe in detail our procedure.

The radial profile of the galaxies can be represented by a generalized exponential law or Sersic law of the form:

$$\mu(r) = \mu_0 + 1.086(r/h)^n, \quad n > 0 \quad (2)$$

where μ_0 is the central surface brightness, h is the scale factor and n is the generalized exponent. The surface brightness profile of disk galaxies and dwarf galaxies fainter than $M_V \sim -17$ are, in general, well fit by a pure exponential law, with $n = 1$ in (2) (Faber & Lin 1993, Binggeli & Cameron 1991, 1993).

The fit to a pure exponential law was used to obtain the extrapolated central surface brightness and the scale length of the LSBD candidates in our sample. For each of the eight isophotal areas given by SExtractor we obtained the surface brightness and the radius using a relation of the form

$$\mu_i = \frac{i}{8}\mu_{peak} + \left(1 - \frac{i}{8}\right)\mu_{lim} \quad i = 0, \dots, 7 \quad (3)$$

where μ_{peak} is the surface brightness at the pixel of maximum intensity, μ_{lim} is the surface brightness at the limiting isophote, and μ_i is the surface brightness at the given isophotal area. Each value of the surface brightness corresponds to a radius $r_i = \sqrt{A_i \epsilon / \pi}$, where $\epsilon = a/b$ is the elongation and A_i is the isophotal area at the i -label given by SExtractor. Using the values for μ_i from (3), we made a least-squares fit to obtain the extrapolated central surface brightness and the scale lengths for each galaxy.

We used the extrapolated central surface brightness and scale length given by the fit as the main parameters to allow a primary cut on the catalogue. All galaxies with central surface brightnesses fainter than 22.5 V mag/arcsec² and scale lengths $h > 3''.0$ and $h > 2''.0$ for the CTIO and

LCO40 observations respectively were selected (note that the seeing strongly affects these structural parameters for $h < 3''$ and $2''$ respectively). This surface brightness cut is similar to that used by Dalcanton et al. (1997) to study the number counts of LSBD in the local universe and is one magnitude fainter than the value used by O’Neil et al. (1997) to search for low-surface brightness galaxies in the Pegasus and Cancer clusters. The first cut on the data selected 777 objects in all fields.

The second cut was done selecting galaxies with a limiting diameter $D_{lim} = 2\sqrt{A_{lim}\epsilon/\pi} \geq 14''$ at the limiting surface brightness of $26 \text{ V mag/arcsec}^2$. The diameter at the limiting isophote (limiting diameter hereafter) can be expressed also by the parameters given by the exponential fit (Allen & Shu 1989):

$$\theta_{lim} = 0.735(\mu_{lim} - \mu_0)10^{0.2(\mu_0 - m_{tot})} \quad (4)$$

where μ_{lim} is the surface brightness at the limiting isophote of $26 \text{ V mag/arcsec}^2$, μ_0 is the extrapolated central surface brightness, and m_{tot} is the total magnitude of the objects. In our case, a diameter of $\gtrsim 14''$ represents well the expected sizes of LSBD that can be detected. This is supported by Monte-Carlo simulations (see next section), which show that the fraction of detected LSBD with exponential profiles with $22.5 \leq \mu_0 \leq 24.5$ ($22.5 \leq \mu_0 \leq 25.5$ for LCO40 fields) and diameters $\geq 14''$ is $f \gtrsim 80\%$ down to $V \sim 20.0$ ($V \sim 22$). The second cut on the data (size limit) limited the sample to 144 LSBD candidates. Each of these galaxies were inspected visually and 84 of them were discarded. We eliminated these galaxies based on the *flag* of the photometric quality (Bertin & Arnouts 1996). We found that all objects with $flag > 0$ have a bright object in their proximity (with the additional contaminating light from the nearby bright source, the false LSBD’s were artificially included in our catalogue). This last cut limited the sample to 60 LSBD candidates. The same selection criteria were used to find LSBD in the two control fields (LCO40) in order to estimate the contribution of background galaxies to the luminosity function. We found only one galaxy in both control fields with $\mu_0 \geq 22.5 \text{ V mag/arcsec}^2$, diameter $\geq 14''$, scale length $h > 2''$. This galaxy seems to be a genuine low-surface brightness galaxy in the field with apparent magnitude $V = 18$ and color $V - I = 1.1$. In addition to the 60 LSBD galaxies, we found five LSBD galaxies in the LCO40 fields with $\mu_0 \geq 22.5 \text{ V mag/arcsec}^2$, scale length $h > 2''$ and diameter $\geq 14''$ at the limiting surface brightness of $\mu_{lim} \geq 26.5 \text{ V mag/arcsec}^2$ (see section 2.7.1).

Table 3 lists the photometric data and the profile fitting parameters of the LSBD detected in the group (the last four lines of the table correspond to the large LSBD namely L01 to L04 - see section 2.7). The data are given as follows: column 1 provides the galaxy identification; columns 2 and 3 list the equatorial coordinates at the epoch 2000.0; columns 4 and 5 show the “total” magnitude (SExtractor “auto” magnitude, not corrected according to the simulations and not corrected by interstellar absorption) in V and the $V - I$ colors within apertures of $7''$ and $4''$ in diameter for CTIO and LCO40 data respectively; columns 6 and 7 list the limiting isophotal diameter and the diameter given by relation (4) at the surface brightness of $26 \text{ V mag/arcsec}^2$; the

extrapolated central surface brightness $\mu_0(V)$ and the scale lengths are given in columns 8 and 9; the next two columns (10 and 11) show the effective radius and mean effective surface brightness; the last column shows the morphological type (see section 3.1). The effective radius in column 10, defined as the radius of the isophote that contains half of the total light, can be represented, in the case of a pure exponential law, by $r_{eff} = 1.668h$ and the mean effective surface brightness (column 11) by $\mu_{eff} = \mu(r_{eff}) = \mu_0 + 1.086(r_{eff}/h)$ (Binggeli & Cameron 1991). The equatorial coordinates in Table 3 (columns 2 and 3) were determined using 20-30 stars from the Guide Star Catalogue present on the images giving an accuracy in the position of less than $2''$.

2.6. Photometric uncertainties and completeness of the sample via Monte Carlo simulations

We performed Monte Carlo simulations in order to determine: *i*) the completeness for point sources; *ii*) the completeness for LSBG galaxies (i.e. the fraction of them detected with the automatic detection described in Section 2.3); and *iii*) the uncertainties in the photometry of the LSBG galaxies. The simulations were performed on the science frames in order to have the same characteristics of a real image (cosmetic defects, crowded images, light gradients, noise and seeing).

We first computed the completeness of the sample by adding point sources constructed from the observed point spread functions and checking the fraction of them we could recover. The results are shown in Figure 3 and quantified in Table 4. From the figure we can see that our completeness limit for point sources with “stellarity index” ≥ 0.9 is $\geq 90\%$ to the limits of ~ 20 and ~ 23 for the CTIO and LCO40 frames respectively.

We then computed the completeness of the sample for galaxies with magnitudes, central surface brightnesses and scale lengths typical of low-surface brightness dwarf galaxies at the redshift of the group. For this we assumed that the LSBG have an exponential profile. For each image, we simulated galaxies with exponential profiles with different scale lengths, central surface brightnesses and random ellipticities. Each image was convolved with a point spread function constructed from bright stars in the frame. The method implemented was the following: *i*) for each bin of central surface brightness we generated 400 randomly distributed disk galaxies in groups of 20 (five for the brightest bins) with magnitudes between 16.0 – 20.0 and 16.0 - 22.0 for the CTIO and LCO40 frames respectively. These galaxies were created using the MKOBJECTS program in the NOAO.ARTDATA package in IRAF; *ii*) we ran the SExtractor program with the same detection parameters previously used for the real-galaxy detection (see section 2.3). Common objects in the input and output catalogues were matched; *iii*) using the eight isophotal areas, for each matched galaxy given by SExtractor, we calculated the central surface brightness, the scale length and the limiting diameter using equations (2) (for $n = 1$), (3) and (4) of section 2.5; *iv*) finally, the photometric and structural parameters were compared with the input parameters.

Table 5 lists the average completeness fraction for LSBG with $22.5 < \mu_0 < 25.5$ mag/arcsec²

($22.5 < \mu_0 < 26.5$ for the LCO40 frames), $16 < V_{tot} < 21$ and $\theta_{lim} > 14''$. The fractional values are the averages over the ranges of surface brightness (per 0.5 bin in magnitude). Figure 4 shows the same results in graphical form. The completeness is, on average, $f \sim 80\%$ in all cases except for the last bins in surface brightness ($24.5 < \mu_0 < 25.5$ and $25.5 < \mu_0 < 26.5$ for CTIO and LCO40 frames respectively). In those cases the completeness fraction is less than 40%. The completeness in magnitude falls abruptly for $V > 20$. Table 6 shows the average differences between input and output magnitudes, central surface brightnesses and scale lengths (in percentage of $(h_{inp} - h_{out})/h_{inp}$). Figure 5 shows differences between input and output magnitudes in a graphical form. The differences in magnitude are lower than 0.3 mag (solid symbols in both panel in Fig. 5) for $\mu_0 < 24.5$ (CTIO) and $\mu_0 < 25.5$ (LCO40). In this interval, the average differences between input and output central surface brightnesses are less than 0.5 V mag/arcsec². For the scale lengths, our simulations show that output values are, on average, larger than input ones by $\sim 20\%$. For the last surface brightnesses bin in the CTIO and LCO40 data, these differences are $\sim 40\%$ and $\sim 30\%$ respectively (last two columns in Table 6). This result shows our limitation in estimating in a correct way the scale length of our real galaxies especially at small sizes. The values for the scale length listed in Table 3 with $h < 5''$ and $M_V > -12.5$ are only upper limits (see also Fig. 8a in section 3.2). In the next section we describe an alternative method used to detect large galaxies with very low surface brightnesses. It increases the completeness fraction in the last bin of central surface brightness to $\sim 80\%$. No galaxies with magnitudes brighter than 18 and central surface brightnesses $\mu_0 > 24.5$ were found in our sample. These objects would have scale lengths $h > 8''$. These have not been found in other surveys either.

2.7. Searching for large low-surface brightness galaxies

2.7.1. Galaxies below the $\mu_{lim} = 26$ in the LCO40 fields

The limiting surface brightness imposed by the central field of $\mu_{lim} = 26$ represents $1.7\sigma_{sky}$ in the LCO40 fields taken in the outskirts of the group. We therefore made an additional search for galaxies with diameters larger than $14''$ but at limiting isophotal level of 26.5 V mag/arcsec² (or $1.2\sigma_{sky}$) only on the LCO40 fields. In this way we discovered five new galaxies that are listed in Table 3 with a “d”, where “d” stands for deep. The inclusion or exclusion of these galaxies in the analysis described below does not change the results.

2.7.2. Large low-surface brightness galaxies in all fields

As described in section 2.3, the sky subtraction was done by taking the median values for image sections of 64×64 pixels and 128×128 pixels in size. This limiting size, used for making the background map could erase any signs of larger galaxies in our frames, if they were present. We then repeated the reduction procedure using background sub-sections of 128 and 256 and re-did searches

for galaxies with larger sizes. This was done by smoothing the images after masking all high-surface brightness objects. The detection was done in the smoothed images and the photometric and structural parameters were obtained in the unconvolved images. The advantage of the smoothing technique used to reduce the pixel-to-pixel noise is that it may be done with a filter that is matched to the shape and size of the galaxy which we are looking for; this produces the maximum gain in signal-to-noise (enhancement of the image) for the targeted galaxies. The original data can provide additional information on any low-surface brightness features detected after smoothing.

The procedure used was the following: *i*) all objects with 3σ above sky were masked and substituted by the appropriate sky noise of each image; *ii*) an additional area around each object in (*i*) was also masked in the same way, to ensure that all high-surface brightness areas of the image were masked. A 2-pixel “growing radius” was used for this purpose (i.e., the radius of each object in (*i*) was incremented by 2 pixel for masking); *iii*) the “clean” image from (*ii*) was convolved with gaussian functions of different widths and for each resulting image we ran SExtractor in order to look for large remaining low-surface brightness objects; *iv*) the photometry of the objects detected in the smoothing images were done in the original frames using the convolved images as templates. At this point, we also did an eye inspection of the images to check if the automatic search with SExtractor had lost any objects.

In this way a number of new very low-surface brightness objects were uncovered in the CTIO frame (four galaxies). No additional galaxies were found in the LCO40 frames at 1σ sky level. The last lines of Table 3 show the photometric and structural parameters for these four galaxies. No color information is available since these were not detected in I. The three panels in Figure 6 exemplify our procedure. The upper-left panel shows the masked image with an extended, low surface brightness galaxy that could not be detected by SExtractor using the procedure in section 2.3 (galaxy L01 in Table 3). The upper-right panel shows the same object after smoothing by a gaussian filter. Finally, the lower panel shows the SExtractor detection on the smoothed image.

One of the detected low-surface brightness object (L02 in Table 3) is very extended and has an irregular morphology and very low-surface brightness. This “cloud” has a size of $\sim 2' \times 1'$ ($10 \times 5 \text{ h}^{-1} \text{ kpc}$), much larger than the value obtained with SExtractor (see Table 3). This “cloud” is located $\sim 10'$ NW of the central galaxy NGC1549. A discussion about the nature of this object is given in section 4.

In order to quantify our ability to detect the extended LSB objects and to evaluate the photometric errors of this technique, we have performed Monte Carlo simulations in a similar way to what was discussed in section 2.6, but applying a smoothing filter. For each image, we applied the method explained above to obtain a smoothed and cleaned frame and to detect extended, LSB in the images with SExtractor. Figure 7 shows a simulated galaxy with $V \sim 18.5$ and $25.5 < \mu_0 < 26.5$. The results of the simulations show that the completeness fractions increase from 40% (obtained with the simulation in section 2.6) to $\sim 80\%$ (with the technique employed here) for galaxies with $24.5 < \mu_0 < 25.5$ (CTIO), $25.5 < \mu_0 < 26.5$ (LCO40), and magnitudes

between $18 < V < 20$. The differences in magnitude (input – output) is $\sigma(\Delta m) < 0.3$ mag (open symbols in figures 4 and 5 respectively). The results of these simulations for the last two bins of surface brightness are quantified in Table 6.

3. Results

Here and in the following sections we will assume that all detected LSBG galaxies in our sample are group members.

3.1. Morphological types of the LSBG galaxies

The LSBG images in the central region of Dorado are of too low resolution to allow a good morphological classification. In this region only a few of the largest galaxies can be classified. However, for the LCO40 data, taken at the outskirts of the group, a classification of all galaxies was attempted (including the 5 LCO40 galaxies with limiting surface brightness 26.5 V mag/arcsec²). Our visual classification of 27 galaxies (9 in the central region, including the large low-surface brightness galaxies) shows that 6 are clumpy, which we classify as dwarf irregular galaxies and 21 have smooth morphology, classified in a broad way as dwarf elliptical galaxies. From the 21 dwarf elliptical galaxies, three, and possibly another 3 in the central region, show bulge and disk (see below). Three of the dwarf irregular galaxies in the LCO40 frames seem to have star forming regions.

3.2. Central surface brightness, scale length and color distributions

Figure 8 shows $\log_{10} h - M_V$ and $\mu_0 - M_V$ diagrams for the 60 LSBG galaxies detected in the region of the Dorado group down to $\mu_{lim} = 26$ V mag/arcsec² after the cuts described in section 2.5. It also shows four additional large low-surface brightness galaxies found with a smoothing technique (see section 2.7) and the five galaxies detected in the LCO40 fields down to $\mu_{lim} = 26.5$ V mag/arcsec² (section 2.7.1). The total magnitudes were corrected by the flux loss by SExtractor (aperture corrections). These values were obtained in the simulations and are quantified in Table 6, section 2.6. The magnitudes were also corrected for interstellar absorption. The absorption correction was obtained from the reddening maps of Schlegel et al. (1998), using the relations $A(V) = 3.1 \times E(B - V)$ and $A(I) = 1.5 \times E(B - V)$ taken from Cardelli et al. (1989). At the position of the group, the absorption correction for the V filter is less than 0.04 mag and for the colors, the correction is less than 0.02 mag. In Figure 8 we plotted also, for comparison, the Local Group (LG) dSph galaxies with $M_V > -16$ (filled pentagons) redshifted to the distance of Dorado. The absolute magnitudes, central surface brightnesses and scale lengths of the LG dSph galaxies were obtained from Lin & Faber (1983), Caldwell et al. (1992), Da Costa (1994) and Irwin &

Hatzidimitriou (1995). As we can see from the plots, several dSphs of the Local Group could be detected at the distance of Dorado, if they were present there. The faintest Local Group dSphs, with absolute magnitudes fainter than $M_V = -11$, like Draco, Carina, Sextans and Ursa Minor, would not be detected at the distance of Dorado.

We find no clear correlation in the $\mu_0 - M_V$ plane (Fig. 8b) and a weak correlation is seen in the scale-length – M_V plane (Fig. 8a). Correlations in these two planes do not have physical meaning since they may be produced by selection effects. The night-sky brightness introduces a strong selection effect and restricts the true determination of the luminosity distribution of galaxies. Both very compact, high-surface brightness objects and extended, very low-surface brightness galaxies are hard to detect. However, the numbers of compact high-surface brightness in groups may be small (see for example Drinkwater et al. 1996).

The faintest LSBG found in Dorado has an absolute magnitude of $M_V = -11.1$ ($V \sim 20.1$), with a central surface brightness of $\mu_0 = 22.9$ V mag/arcsec² and a scale length $h = 2.6''$ ($\sim 0.3 h^{-1}$ kpc). The largest LSBG galaxy ($D_{26} \sim 69''$) has a scale length of $h = 11.1''$ ($0.9 h^{-1}$ kpc), $M_V = -15.5$ and $\mu_0 = 22.7$ V mag/arcsec². The colors inside a diameter of $7''$ (CTIO) and $4''$ (LCO40) of the 65 LSBG galaxies detected in Dorado with a color information vary from $-0.3 < V - I < 2.3$ with a peak at $V - I = 0.98$ (see Figure 9).

We have obtained the surface brightness profiles of the 65 LSBG using the task ELLIPSE in the STSDAS package inside IRAF. We then used the procedure described in section 2.5 to obtain the extrapolated central surface brightness and scale lengths by a least squares fitting procedure (we used here only the outer parts of the profiles to avoid the region affected by seeing). The comparison between the results given from the SExtractor areas (see section 2.5) and by ELLIPSE are similar (within 0.2 V mag/arcsec² for μ_0 and within 20% for the scale length). These results are also in good agreement with the Monte Carlo simulations (see section 2.6). Figure 10 shows the surface brightness profiles for the 65 LSBG galaxies (we do not include the four large low-surface brightness galaxies listed at the end of Table 3 because of the poor fit to the data). In this figure the x-axis is the semi-major axis of the elliptical isophote. As we can see in the figure, all LSBG follow well an exponential profile characteristic of disk-only galaxies, outside the area strongly affected by seeing ($r > 4''$). However, a few of the galaxies show a prominent bulge, e.g. 3330-10 and 1116-11. In the central field - CTIO - the large pixel size ($\sim 2''$) could be masking the presence of a bulge, if it exists. However, three galaxies in the CTIO frame hint and evidence for a bulge (4536-01, 5622-01 and 7731-01).

3.3. Color profiles

In order to analyze the color profiles of the 65 LSBG galaxies we have obtained their magnitudes within concentric circles of growing radii (starting from $3.5''$ and $2''$ radius for CTIO and LCO40 frames respectively) using SExtractor. For each galaxy, the profile for the I band was subtracted

from that for the V band to form the color profile. Figure 11 shows the color profiles of the 65 LSBD for which color information is available. Most of the galaxies show flat color profiles, i.e. very small gradients with an average for all galaxies of $d[V - I]/dR = -0.014 \pm 0.052$. However, in a few cases we measured a small inclination in the profiles. Galaxies 874-01, 1843-01, 3747-01, 1064-03 and 2674-06 become redder with increasing radius. This effect was also found by Patterson & Thuan (1996) for some dwarf irregular galaxies and by Bremnes et al. (1998, 1999) for low-surface brightness galaxies in the M81 and M101 groups. Other galaxies like 873-01, 2374-01, 4136-01, 5012-01 and 7022-01 become bluer with increasing radius. These results are discussed in section 4.

3.4. Projected number density of the LSBD galaxies

Figure 12 shows the logarithm of the surface number density (in units of $h^2 \text{ kpc}^{-2}$) as a function of the distance to the group center (the centroid of the two central galaxies) for all LSBD galaxies detected in the region of Dorado (the five LSBD galaxies detected in LCO40 at $\mu_{lim} = 26.5$ V mag/arcsec² were not included in this plot, but if they are included the result is unchanged). The data for the central region (CTIO) was divided in bins of $\sim 75 \text{ h}^{-1} \text{ kpc}$ (0.25 degree) and normalized by the corresponding area. For the LCO40 data each field was plotted as one point in Fig. 12, where the number of galaxies was normalized by the total area used in each field.

From this figure we can see that there is a clear central concentration of LSBD, inside a radius of $\sim 250 \text{ h}^{-1} \text{ kpc}$ (~ 0.8 deg). At a radius $r > 250 \text{ h}^{-1} \text{ kpc}$ the projected number density is similar to the values found in our control fields (~ 7 galaxies per square degree) and by Dalcanton et al. (1997). At $\sim 400 \text{ h}^{-1} \text{ kpc}$ (~ 1.3 deg) and $\sim 700 \text{ h}^{-1} \text{ kpc}$ (~ 2.1 deg) from the center we found a slight enhancement in the projected number density of LSBD galaxies. These density enhancements could be associated to the early-type galaxies NGC1536 (field D05) and NGC1574 (field D11). Two of the three galaxies in the D11 field that may be associated to NGC1574 galaxy are dwarf irregulars and one is a dwarf elliptical galaxy. Figure 13 shows the projected distribution of all bright galaxies with known redshift, like Fig. 1, but including the LSBD galaxies detected in our survey. From the figure we can see that the majority of the galaxies lie in the central region and five of the nine galaxies in the outskirts of the group seem to be associated to bright early-type galaxies.

We fit an exponential profile to the data shown in Figure 12 (for the three points with $r \leq 250 \text{ h}^{-1} \text{ kpc}$) in order to find the scale size and the central (extrapolated) galaxy number density of the LSBD galaxy. We find a scale size of $270 \text{ h}^{-1} \text{ kpc}$ (~ 0.9 deg). Alternatively, if we fit a power law of the type $\Sigma \propto r^{-\beta}$ within a radius of $250 \text{ h}^{-1} \text{ kpc}$, we find that $\beta = -1.09 \pm 0.32$.

4. Discussion and Summary

4.1. Colors and color profiles

The colors and color profiles of the LSBD may give us information on the stellar content and other physical parameters as a function of radius (for example, metallicity). The color distribution of the LSBD candidates of the Dorado group range from $-0.3 < V - I < 2.3$ with a peak at $V - I = 0.98$ (Figure 9). The color range and peak value are in a good agreement with the values obtained for the LSBD in the Virgo and Fornax clusters (Impey et al. 1988, Bothun et al. 1991) and in the Pegasus and Cancer spiral-rich clusters (O’Neil et al. 1997). About half the LSBD population of Dorado is composed of blue galaxies with $V - I < 1$ and 12% are very blue with $V - I < 0.5$. These values are comparable, in percentage, to those found by O’Neil et al. (1997) in the Pegasus and Cancer nearby groups. As pointed out by these authors, the blue LSBD are important because of the restrictions imposed on their star formation histories and also because they could be the local counterparts of the distant faint blue galaxies.

The average flat color profiles found for the LSBD in Dorado shown in section 3.3 suggest that there is no star formation or, if it exists, it is very weak. The very blue colors in some galaxies is restricted to the central regions and they can be explained by the existence of a sporadic burst with a constant, but very low, star formation rate. The star formation decreases or disappears in the outer parts of the galaxies.

Rich clusters like Coma do not contain a large population of blue LSBD objects most probably because the evolution of these galaxies is accelerated and they could not survive a long time in such a hostile environment. The color distribution of the Coma dwarf galaxies peaks at $B - R = 1.4$ and at fainter magnitudes they become bluer, to a mean $B - R$ of 1.15 (Secker et al. 1997). These two peaks are much redder than the peak in the Dorado group ($V - I = 0.98$, corresponds to a typical $B - R \sim 0.5$). This is expected, since the Dorado group has a very low density environment of bright galaxies.

Blue LSBD have been identified and are well studied in a number of nearby groups and in the field (e.g. McGaugh & Bothun 1994, de Block et al. 1995, Impey et al. 1996, Pildis et al. 1997, O’Neil et al. 1997). However, we still lack good information on red LSBD galaxies since most of the previous works were done with photographic plates. Practically all of the LSBD observed in photographic surveys are blue since photographic data are biased towards finding blue objects. About 12% of the LSBD sample in this work shows colors $V - I > 1.5$ mag. For some galaxies the colors are very red (e.g. 779-01, 4536-01 and 3330-10 with $V - I > 1.8$) with a flat color profile (see Fig. 11). The red colors found for these galaxies could not be explained by photometric errors (the errors are < 0.3 mag, see section 2.6), by interstellar absorption (the color correction is less than 0.02 mag) or by internal reddening (there is no evidence for a high dust content in the LSBD galaxies, O’Neil et al. 1997).

Detection of very red LSBD galaxies in nearby poor groups is not new. Recently, in a survey

of low-surface brightness galaxies in the Pegasus and Cancer clusters taken by O’Neil et al. (1997), a significant population of red LSB galaxies was discovered. About 20% of the galaxies in their sample have colors $V - I > 1.5$. The percentage of red galaxies in Dorado is similar ($\sim 12\%$). One probable scenario to explain the colors of these galaxies, discussed by O’Neil et al. (1997), is that these objects “underwent starburst early in their existence, consuming most of the galaxies gas and leaving them with an old stellar population”.

Some examples of very red LSB ($V - I > 1.8$) in the Dorado group are 779-01, 4536-01 and 3330-10. Due to the poor resolution of the CTIO image, it was impossible for us to obtain a morphological classification for 779-01 and 4536-01. However, the 3330-10 galaxy was classified as a dIrr galaxy. This galaxy is a special case because it is very red ($V - I \sim 2.2$) and shows an irregular morphology, with a large disc and strong bulge. A number of very red low surface brightness galaxies detected by O’Neil et al. (1997) were recently surveyed in HI by O’Neil et al. (2000). They showed that a few of them are gas-rich low-surface brightness galaxies with no massive star formation and with $M_{HI}/L_B > 9$. We have no information about the HI content of the 3330-10 galaxy and we can only speculate that this galaxy could have properties similar to those of the galaxies discovered by O’Neil et al. (2000) in their survey. Additional HI observations are needed to confirm this point.

4.2. Projected number density of the LSB galaxies

The clustering properties of the dwarf galaxy population is an important tool for cosmology. The space distribution of the dwarf satellites around bright galaxies could indicate how luminous and dark material are distributed at different scales. Moreover it may be a tracer of the dynamical evolution of the dark halos around bright galaxies.

As determined in Section 3.4, the central galaxy concentration dies off outside a distance to the group center of $\sim 250 \text{ h}^{-1} \text{ kpc}$. The radial distribution (Fig. 12) is in general agreement with the results obtained by Mulchaey & Zabludoff (1999) for five X-ray groups, although they cannot be compared in detail given the different magnitudes considered in this and their studies (we consider galaxies with $-16 < M_V < -11$ and they considered galaxies with $-17 < M_V < -15$ for $H_0 = 75 \text{ km s}^{-1} \text{ Mpc}^{-2}$ and $V - R \sim 0.6$).

It is well known that dwarf elliptical galaxies show a stronger clustering around early-type galaxies (e.g. Vader & Sandage 1991) than around late-type galaxies (e.g. Lorrimer et al. 1994) and are more common in large and rich environments. The Dorado group has two bright early-type galaxies (one E1 and one S0) in the center, separated by only $58 \text{ h}^{-1} \text{ kpc}$, and has no other prominent early-type object in its outskirts. In a radius of $\sim 0.5 \text{ h}^{-1} \text{ Mpc}$ from the central galaxies, only four galaxies with absolute magnitudes brighter than $M_V = -20$ are present, and they are all late-type objects. In order to analyze if the LSB galaxies detected in Dorado group are associated to the bright central early type NGC1549 and NGC1553 galaxies of Dorado or to the potential well

of the group, we plotted the distribution of all LSBd detected in our survey around three different positions: 1) the E1 galaxy NGC1549, 2) the centroid of the two central group galaxies and 3) the S0 galaxy NGC1553. We found no significant difference between these three plots. The central concentration detected suggests the galaxies are true dwarf galaxies of the Dorado group but we cannot decide from the exercise above if they belong to the group or to the two central early-type galaxies.

To further test this point, we compared our result with those obtained for satellites of isolated bright elliptical galaxies. The study of Vader & Sandage (1991) found that the density of satellites, if fit to a function $\Sigma \propto r^{-\beta}$, with $\beta = -1.22$. This agrees with our value of -1.09 . Furthermore, the distribution of satellites around the center of Dorado is similar in extent to that found around the the X-ray bright elliptical galaxy NGC 1132 studied by Mulchaey and Zabludoff (1999). These comparisons would seem to suggest that the LSBd galaxies in the Dorado group are most probably physically associated with the two central galaxies. However, since these galaxies strongly dominate the potential well of the group, this may be equivalent to saying that the satellites we measured are associated with the overall potential of the group. An alternative interpretation of these results would be that isolated elliptical galaxies and groups have similar distributions of satellites around them perhaps because all bright field elliptical galaxies may be merged groups (as may be the case for NGC 1132 discussed by Mulchaey and Zabludoff 1999).

4.3. LSBd, tidal interacting feature or Galactic cloud?

We discovered an extended low-surface brightness “cloud” $\sim 10'$ (about $50 \text{ h}^{-1} \text{ kpc}$) to the NW of the central NGC1549 galaxy (galaxy L02 in Table 3, see Section 2.7.2). The object, shown in Fig. 14, has a smooth appearance, like a dwarf elliptical galaxy. However, it is much larger than all the other satellite candidates ($\sim 10 \times 5 \text{ h}^{-1} \text{ kpc}$) and it is very close to one of the central galaxies.

Bremnes et al. (1998) has detected several low-surface brightness clouds in the direction of M81 which overlap with detections in the IRAS $100 \mu\text{m}$ map, suggesting that these may indeed be cirrus structures in our own Galaxy. However, in the case of Dorado, the IRAS $100 \mu\text{m}$ map of the region shows no similar features. Moreover, the “cloud” in Dorado is much closer to a bright galaxy than in the case for the clouds in the M81 group.

An alternative explanation would be that this object is the residual of a past galaxy-galaxy interaction or a disrupted dwarf galaxy like Sagittarius in the Local group. Higher resolution imaging of this object may reveal its nature.

4.4. Summary

Summarizing, we have detected 69 low-surface brightness dwarf galaxies as candidate dwarf members of the nearby group of galaxies Dorado. Our CCD survey covered ~ 2.6 square degrees of the group. The galaxies were chosen based on their sizes and magnitudes at the average limiting isophote of $26 \text{ V mag/arcsec}^2$. We showed, using Monte Carlo simulations, that we are able to detect possible dwarf members in Dorado with $-10.5 > M_V > -17$ with $22.5 < \mu_0 < 25.5 \text{ V mag/arcsec}^2$ with a completion fraction $f > 80\%$. Four new large low-surface brightness galaxies previously undetected by standard techniques were detected using a smoothing technic. One of these galaxies is a large low-surface brightness “cloud” with an irregular shape much more extended than the other dwarf galaxies in the survey. The color distribution for the 65 LSB galaxies with color information varies from very blue to very red with a peak at $V - I = 0.98$. The color profiles of the galaxies show very small gradients (on the order of the photometric errors). In some cases we measured a small inclination in the profiles. The reddest galaxy (3330-10) shows an irregular morphology, a strong bulge, a large halo and a flat color profile. This galaxy could be a HI-rich galaxy like others of the same type found in the Pegasus and Cancer clusters by O’Neil et al. (2000). The projected surface density shows a significant excess of LSB galaxies within $\sim 250 \text{ h}^{-1} \text{ kpc}$ ($\sim 0.8 \text{ deg}$) from the center of the group. Comparisons with others results obtained from X-ray groups and for the isolated elliptical galaxy NGC1132 suggest that the Dorado LSB are probably physically associated with the overall potential well of the group.

The authors are grateful to the Directors of CTIO and Las Campanas Observatory for generous allocation of telescope time. ERC acknowledges support for this work provided by FAPESP PhD fellowship Nr. 96/04246-7. CMdO is grateful to E. Bertin for several discussions about the use of the SExtractor package. L.I. was supported partially by Proyecto FONDECYT Nr. 8970009 and a Guggenheim Foundation award. This work benefitted from the use of the NASA/IPAC Extragalactic Database (NED), which is operated by the Jet Propulsion Laboratory, California Institute of Technology, under contract with the National Aeronautics and Space Administration.

REFERENCES

- Allen, R. J. & Shu, F. H. 1979, *ApJ*, 277, 67
- Bertin, E. & Arnouts, S., 1996, *A&AS*, 117, 393
- Binggeli, B. & Cameron, L. M. 1991, *A&A*, 252, 27
- Binggeli, B. & Cameron, L. M. 1993, *A&AS*, 98, 297
- Bothun, G. D., Impey, C. D. & Malin, D. F. 1991, *ApJ*, 376, 404
- Bremnes, T., Binggeli, B. & Prugniel, P. 1998, *A&AS*, 129, 1

- Bremnes, T., Binggeli, B. & Prugniel, P. 1999, A&AS, 137, 337
- Caldwell, N., Armandroff, T. E., Seitzer, P. & Da Costa, G. S. 1992, AJ, 103, 840
- Cardelli, J. A., Clayton, G. C. & Mathis, J. S. 1989, ApJ, 345, 245
- Carignan, C. & Freeman, K. C. 1988, ApJ, 332, L33
- Da Costa, D. G. 1992, in *Dwarf Galaxies*, eds. by G. Meylon et al., ESO/OHP Workshop Proceedings Nr. 49, p. 221
- Dalcanton, J. J., Sperel, D. N., Gunn, J. E., Schmidt, M. & Schneider, D. P. 1997, AJ, 114, 635
- de Block, W., van der Hulst, J. & Bothun, G. 1995, MNRAS, 274, 235
- de Vaucouleurs, G., 1975, in *Star and Stellar System*, edited by A. Sandage, M. Sandage, and J. Kristian (University of Chicago, Chicago), Vol.9, p. 557.
- Drinkwater, M. J., Currie, M. J, Young, C. K., Hardy, E. & Yearsley, J. M. 1996, MNRAS, 279, 595
- Faber, S. M. & Lin, D. N. C. 1983, ApJ, 266, L17
- Ferguson, H. 1989, AJ, 98, 367
- Ferguson, H.C. & Sandage, A., 1990, AJ, 100, 1
- Ferguson, H.C. & Sandage, A., 1991, AJ, 101, 765
- rebel, E. K. 2000, astro-ph/0005296
- Huchra, J. P. & Geller, M. J. 1982, ApJ, 257, 423
- Impey, C., Bothun, G. & Malin, D. 1988, ApJ, 330, 634
- Impey, C., Sprayberry, D., Irwin, M. & Bothun, G. 1996, ApJS, 105, 209
- Impey, C. & Bothun, G. 1997, ARA&A, 35, 267
- Infante, L. 1987, A&A, 183, 177
- Infante, L. & Pritchett, C. 1992, ApJS, 83, 237
- Irwin, M & Hatzidimitriou, D. 1995, MNRAS, 277, 1345
- Jerjen, H., Binggeli, B. & Freeman, K. C. 2000, AJ, 119, 593
- Kron, . 1980, ApJS, 43, 305
- Landolt, A.U., 1992, AJ, 104, 340.

- Lin, D. N. C. & Faber, S. M. 1983, *ApJ*, 266, 21
- Lorrimer, S. J., Frenk, C. S., Smith, R. M., White, S. D. M. & Zaritsky, D. 1994, *MNRAS*, 269, 696
- Maia, M. A., da Costa, L. N. & Latham, D. W. 1989, *ApJS*, 69, 809
- Marzke, R. O., da Costa, L. N., Pellegrini, P. S., Willmer, C. N. A. & Geller, M. J. 1998, *ApJ*, 503, 617
- McGaugh, S. & Bothun, G. 1994, *AJ*, 104, 530
- Mulchaey, J. S. & Zabludoff, A. I. 1999, *ApJ*, 514, 133
- O’Neil, K., Bothun, G. D., Schomber, J., Cornell, M. E. & Impey, C. D. 1997, *AJ*, 114, 2448
- O’Neil, K., Bothun, G. D. & Schomber, J. 2000, *AJ*, 119, 136
- Patterson, R. J. & Thuan, T. X. 1996, *ApJS*, 107, 103
- Pildis, R. A., Schomber, J. M. & Eder, J. A. 1997, *ApJ*, 481, 157
- Pritchett, C. & van den Bergh, S. 1999, *AJ*, 118, 883
- Sandage, A., Binggeli, B. & Tammann, G.A. 1985, *AJ*, 90, 1759
- Shakhbazian, R.K. 1957, *Astron. Tsirk.*, 177, 11.
- Schlegel, D. J., Finkbeiner, D. P. & Davis, M. 1998, *ApJ*, 500, 525
- Secker, J. & Harris, W. E. 1997, *PASP*, 109, 1364
- Secker, J., Harris, W. E. & Plummer, J. D. 1997, *PASP*, 109, 1377
- Thompson, L. A. & Gregory, S. A. 1993, *AJ*, 106, 2197
- Vader, . & Sandage, A. 1991, *ApJ*, 379, L1
- van den Bergh, S. 1999, *A&A Rev.*, 9, 273

Fig. 1.— Locations and sizes of the observed CCD frames in the region of the Dorado group. The small squares indicate the LCO40 frames ($24' \times 24'$) and the large square the CTIO frame ($1.15^\circ \times 1.15^\circ$). The triangles indicate all galaxies with known velocities $cz < 2000$ km/s, taken from the NED. North is up and East is to the left.

Fig. 2.— A V image of the central region of the Dorado group ($\approx 1^\circ \times 1^\circ$) taken with the 0.9 m Schmidt telescope at CTIO, Chile. The brightest galaxies in the frame are identified by their NGC or IC numbers. At the bottom of the figure, a mosaic of selected low-surface brightness dwarf galaxies detected in this region is shown. The small squares in the image indicate the location of the galaxies in the area. The photometric and profile fit parameters of these galaxies are listed in Table 3 (see section 2.5).

Fig. 3.— Completeness fraction versus the input total magnitudes for the simulated point sources. The completeness limit for point sources with “stellarity index” ≥ 0.9 is ~ 20.5 for the CTIO frame (upper panel) and ~ 23 for LCO40 frames (lower panel).

Fig. 4.— Completeness fraction versus the input total magnitudes for LSBD simulated galaxies added to the observed frames. The upper and lower panels show the results for the simulations done using the CTIO and LCO40 frames respectively.

Fig. 5.— Differences between the input and output magnitudes obtained from the LSBD Monte Carlo simulations for the fields D01 (upper panel) and D04 (lower panel). In the upper panel (CTIO), $\sigma(\Delta m) < 0.3$ mag ($\Delta m = m_{inp} - m_{out}$) for LSBD with $22.5 < \mu_0 < 24.5$ and $16 < V_t < 21$ (completeness $f > 80$). In the lower panel (LCO40), $\sigma(\Delta m) < 0.3$ for LSBD with $24.5 < \mu_0 < 25.5$ and $18 < V_t < 20$ (completeness $f > 80$). No real galaxies were found in the last bins of surface brightness for $V < 18$. We, therefore, do not plot the corresponding simulations in this figure to avoid confusion.

Fig. 6.— Extended LSBD detected using the smoothing technique. The upper left panel shows the masked image of a galaxy that could not be found by SExtractor at a first pass (section 2.3). The upper right panel shows the smoothed image of the same galaxy after filtering. This galaxy has a magnitude of 18.5, a scale length $h=13.2''$ and a central surface brightness $\mu_0 = 24.8$ V mag/arcsec² (see galaxy L01 in Table 3).

Fig. 7.— Simulated galaxy with $V \sim 18.5$ and $25.5 < \mu_0 < 26.5$ in one of the LCO40 fields (upper left panel). All high-surface brightness objects with a threshold over 3σ are masked (upper right panel). The smoothing filter is applied in order to enhance the galaxies that are at the limit of detection (lower left panel). After smoothing, SExtractor is run in order to detect the extended LSBD (lower right panel). At the limit of detectability of our images, the completeness increases to $\sim 80\%$, using the technique (open circles in figures 4 and 5) .

Fig. 8.— Extrapolated central surface brightness (lower panel) and scale length (upper panel) versus total magnitude for LSBD galaxies detected in the Dorado group region with $\mu_0 > 22.5$ V

mag/arcsec², $h \geq 2''$ ($3''$ for the CTIO frame) and diameter $\geq 14''$. The open stars and triangles are the LSBG galaxies detected in the CTIO and LCO40 frames respectively. The open circles are the large low-surface brightness galaxies detected using the smoothing method of section 2.7. For comparison, we mark in the plot the Local Group dSphs galaxies (filled symbols) redshifted to the Dorado distance ($17.2 h^{-1}$ Mpc). The dashed lines are the central surface brightness and scale length cuts used to select the LSBG ($22.5 \text{ mag/arcsec}^2$ and $3''$ respectively). The solid lines represent the limiting diameter given by equation (4) with $\mu_{lim} = 26 \text{ mag/arcsec}^2$ and by the relation between the total magnitude, central surface brightness and the scale length for galaxies with exponential profiles ($m_t = \mu_0 - 5 \log(h) - 2.5 \log(2\pi)$)

Fig. 9.— Histogram of the color distribution of the 65 LSBG galaxies with a color information. The LSBG galaxies in Dorado show colors between $-0.3 < V - I < 2.3$ with a peak at $V - I = 0.98$.

Fig. 10.— Surface brightness profiles of the 65 LSBG galaxies detected in the region of the Dorado group (V filter). The dashed lines represent the exponential fits as described in the text. The radii are the semi-major axis of the elliptical apertures of the galaxies.

Fig. 11.— Radial color profiles $V - I$ for the 65 LSBG. The color profiles were constructed subtracting the profile for the I band from that for the V band. The majority of the galaxies show a flat color profile with a gradient $d[V - I]/dR = -0.014 \pm 0.052$.

Fig. 12.— Surface density as a function of the radius (in logarithmic scales) for all LSBG galaxies detected in the region of the Dorado group. The data for the central region was divided in bins of $\sim 75 h^{-1}$ kpc (0.25 degree). The radial distance was measured from the centroid of the two central group galaxies NGC1549 and NGC1553.

Fig. 13.— Projected distribution of all bright galaxies with known redshift, like Fig. 1, but including the LSBG galaxies detected in our survey (small circles).

Fig. 14.— CCD Image of the extended low-surface brightness “cloud” located $\sim 10'$ NW from the central galaxy NGC1549. The size of the “cloud” is $\sim 2' \times 1'$ ($10 \times 5 h^{-1}$ kpc). The size of the figure is $8' \times 8'$. North is up, East is to the left.

Table 1. Observation log

Field Id	$\alpha(2000)$ <i>h m s</i>	$\delta(2000)$ <i>° ' "</i>	Filters	Exposure [sec]	A_{tot} [arcmin ²]	A_{used} [arcmin ²]
(1)	(2)	(3)	(4)	(5)	(6)	(7)
D01	4 16 00.5	-55 42 03	V,I	6 × 600	4163.86	3634.79
D02	4 16 02.8	-55 01 41	V,I	3 × 1200	534.42	481.79
D03	4 16 00.5	-54 36 15	V,I		535.52	488.69
D04	4 15 54.4	-53 56 06	V,I		532.11	482.58
D05	4 12 06.3	-56 33 44	V,I		537.11	492.29
D06	4 11 45.1	-57 18 45	V,I		540.61	516.76
D07	4 22 20.6	-55 38 43	V,I		537.93	499.00
D08	4 09 24.4	-55 30 09	V,I		539.00	492.89
D09	4 28 01.3	-55 36 06	V,I		539.84	502.28
D10	4 02 17.4	-55 22 07	V,I		538.46	481.53
D11	4 23 26.4	-56 40 44	V,I	3 × 900	536.88	486.64
B3	3 38 25.3	-25 15 05	V,I	3 × 1200	517.42	451.65
B4	3 38 22.5	-49 59 24	V,I		536.16	477.55

Note. — D01: CTIO observation; D02 to D11 and B3, B4: LCO40 observations

Table 2. Transformation Equations

Run (1)	Night (2)	Transformation equations ^(a) (3)	rms (4)
CTIO	Nov-1-96	$V = v - 4.904 \pm 0.019 - 0.164 \pm 0.015 \cdot X_v - 0.035 \pm 0.003 \cdot (V - I)$	0.022
	Nov-2-96	$I = i - 5.487 \pm 0.013 - 0.038 \pm 0.010 \cdot X_i + 0.004 \pm 0.002 \cdot (V - I)$	0.019
LCO40	Dec-2-96	$V = v - 3.456 \pm 0.010 - 0.150 \pm 0.009 \cdot X_v - 0.057 \pm 0.003 \cdot (V - I)$	0.021
		$I = i - 3.848 \pm 0.009 - 0.104 \pm 0.008 \cdot X_i + 0.039 \pm 0.003 \cdot (V - I)$	0.018
	Dec-3-96	$V = v - 3.490 \pm 0.009 - 0.118 \pm 0.006 \cdot X_v - 0.053 \pm 0.001 \cdot (V - I)$	0.015
		$I = i - 3.909 \pm 0.008 - 0.048 \pm 0.006 \cdot X_i + 0.037 \pm 0.001 \cdot (V - I)$	0.012
	Dec-4-96	$V = v - 3.437 \pm 0.013 - 0.173 \pm 0.009 \cdot X_v - 0.059 \pm 0.002 \cdot (V - I)$	0.023
		$I = i - 3.805 \pm 0.019 - 0.121 \pm 0.014 \cdot X_i + 0.034 \pm 0.004 \cdot (V - I)$	0.020
Dec-5-96	$V = v - 3.458 \pm 0.016 - 0.153 \pm 0.012 \cdot X_v - 0.057 \pm 0.003 \cdot (V - I)$	0.016	
	$I = i - 3.792 \pm 0.023 - 0.129 \pm 0.016 \cdot X_i + 0.039 \pm 0.005 \cdot (V - I)$	0.023	
Dec-6-96	$V = v - 3.438 \pm 0.011 - 0.155 \pm 0.008 \cdot X_v - 0.062 \pm 0.004 \cdot (V - I)$	0.013	
	$I = i - 3.885 \pm 0.018 - 0.079 \pm 0.014 \cdot X_i + 0.044 \pm 0.007 \cdot (V - I)$	0.020	

^(a)The instrumental magnitudes were normalized to 1 second.

Table 3. Photometric data and profile fit parameters of LSBD galaxies in Dorado group

ID	$\alpha(2000)$ [^h ^m ^s]	$\delta(2000)$ [[°] ['] ^{''}]	$V^{(a)}$ [mag]	$(V - I)^{(a)}$ [mag]	D_{26} [^{''}]	θ_{26} [^{''}]	$\mu_0(V)$ [mag/ \square'']	h [^{''}]	r_{eff} [^{''}]	$\mu_{eff}(V)$ [mag/ \square'']	Type
(1)	(2)	(3)	(4)	(5)	(6)	(7)	(8)	(9)	(10)	(11)	(12)
279-01	4 17 09.9	-56 11 51	19.73	0.31	14.1	16.5	23.5	3.5	5.9	25.3	
377-01	4 12 23.7	-56 11 12	18.50	0.95	16.5	18.6	22.7	3.0	5.1	24.5	
666-01	4 19 23.8	-56 07 57	19.16	0.58	16.4	19.4	23.9	5.1	8.5	25.7	
779-01	4 14 02.3	-56 07 38	19.74	2.08	14.4	15.6	23.6	3.6	5.9	25.4	
873-01	4 17 09.4	-56 06 37	19.42	0.66	16.5	22.2	24.6	8.7	14.5	26.4	dE
874-01	4 18 15.4	-56 06 20	20.00	1.43	14.5	16.9	24.1	4.8	8.0	25.9	
972-01	4 17 47.1	-56 05 49	19.47	1.80	14.9	17.2	23.0	3.1	5.2	24.8	
1639-01	4 16 59.0	-56 00 49	18.75	0.82	18.7	21.7	23.5	4.7	7.8	25.3	dE
1709-01	4 14 38.8	-56 00 39	18.96	0.76	16.9	20.5	24.0	5.6	9.4	25.8	
1746-01	4 12 31.7	-56 00 12	19.18	1.42	14.1	16.7	23.7	4.0	6.7	25.6	
1843-01	4 18 45.5	-55 58 57	19.64	0.64	15.2	17.3	24.2	5.2	8.7	26.0	
2318-01	4 17 09.3	-55 55 10	19.70	1.15	14.1	16.0	23.2	3.1	5.2	25.0	
2347-01	4 15 04.5	-55 56 16	18.27	0.51	32.0	39.5	23.0	7.2	12.0	24.8	dIrr
2408-01	4 16 26.9	-55 54 42	19.98	1.03	14.2	15.5	23.9	4.0	6.6	25.7	
2851-01	4 17 44.2	-55 51 23	18.99	1.54	20.8	20.4	23.5	4.4	7.4	25.3	
2915-01	4 15 39.0	-55 51 09	19.31	0.89	15.1	16.3	23.2	3.2	5.3	25.0	
2982-01	4 12 15.6	-55 52 06	16.77	0.75	35.9	39.4	22.5	6.1	10.2	24.3	dE
3625-01	4 13 58.6	-55 46 15	19.70	1.14	15.3	16.4	23.2	3.2	5.3	25.0	
3672-01	4 18 00.5	-55 45 06	19.71	1.30	15.4	16.6	23.8	4.1	6.9	25.6	
3714-01	4 16 20.3	-55 45 09	19.20	0.31	15.6	18.2	23.3	3.6	6.1	25.1	
3747-01	4 15 31.2	-55 44 54	19.84	1.57	17.0	17.3	23.7	4.1	6.8	25.5	
3774-01	4 18 04.6	-55 45 26	17.45	0.84	34.3	40.8	24.0	11.3	18.8	25.8	dE
3829-01	4 16 29.7	-55 44 10	18.69	0.98	14.9	14.9	23.5	3.3	5.5	25.4	
4045-01	4 19 16.6	-55 41 33	19.81	0.91	15.4	19.1	23.9	5.0	8.3	25.7	
4136-01	4 16 15.1	-55 41 51	18.72	0.07	18.2	20.1	24.2	6.2	10.3	26.0	
4302-01	4 14 09.0	-55 42 25	15.74	0.85	68.9	69.6	22.7	11.3	18.9	24.5	dE
4429-01	4 19 29.4	-55 39 00	18.38	0.85	22.4	26.8	23.9	7.0	11.7	25.7	dE
4488-01	4 13 24.8	-55 38 53	19.62	0.88	15.4	17.4	24.2	5.2	8.8	26.0	dE
4536-01	4 17 11.5	-55 38 10	19.66	2.07	15.8	16.7	23.0	3.0	5.1	24.8	
4598-01	4 14 52.7	-55 38 09	19.44	0.85	15.9	15.5	23.6	3.5	5.8	25.4	
4814-01	4 14 40.5	-55 36 02	19.11	0.99	14.1	17.0	23.5	3.7	6.1	25.3	

Table 3—Continued

ID	$\alpha(2000)$ [^h ^m ^s]	$\delta(2000)$ [[°] ['] ^{''}]	$V^{(a)}$ [mag]	$(V - I)^{(a)}$ [mag]	D_{26} [^{''}]	θ_{26} [^{''}]	$\mu_0(V)$ [mag/ [□] '']	h [^{''}]	r_{eff} [^{''}]	$\mu_{eff}(V)$ [mag/ [□] '']	Type
(1)	(2)	(3)	(4)	(5)	(6)	(7)	(8)	(9)	(10)	(11)	(12)
5012-01	4 16 00.4	-55 34 06	19.04	1.14	15.1	14.4	24.2	4.4	7.4	26.1	
5192-01	4 16 22.9	-55 32 29	19.96	1.03	15.3	14.8	23.5	3.2	5.3	25.3	
5242-01	4 18 08.6	-55 32 08	19.11	0.93	16.7	17.8	23.0	3.2	5.3	24.8	
5622-01	4 14 55.0	-55 29 16	19.06	1.01	16.5	17.5	23.0	3.1	5.2	24.8	
5894-01	4 16 09.1	-55 27 33	19.37	0.41	18.2	22.5	23.9	6.0	10.0	25.8	
5923-01	4 18 37.1	-55 26 52	19.54	1.21	14.3	15.5	23.7	3.6	6.0	25.5	
6672-01	4 16 48.3	-55 16 05	19.13	1.23	16.1	19.3	23.1	3.6	6.0	24.9	
6740-01	4 19 26.9	-55 16 11	18.85	0.12	20.8	21.0	22.6	3.4	5.6	24.4	
6854-01	4 14 09.8	-55 19 22	19.34	1.25	16.9	17.3	23.5	3.7	6.2	25.3	
6942-01	4 14 44.6	-55 18 25	19.89	1.52	14.5	17.2	24.0	4.8	8.0	25.9	
7022-01	4 12 53.3	-55 19 30	19.29	0.24	14.9	18.7	23.7	4.4	7.4	25.5	
7328-01	4 12 56.6	-55 22 34	18.99	0.71	18.9	20.5	22.7	3.4	5.7	24.5	
7330-01	4 16 07.0	-55 22 10	18.26	0.25	25.9	28.9	24.4	9.9	16.6	26.2	dE
7392-01	4 12 18.4	-55 22 54	18.64	1.37	24.4	26.1	22.8	4.4	7.3	24.6	
7493-01	4 14 20.7	-55 23 36	19.79	1.36	15.2	16.4	23.7	3.8	6.4	25.5	
7547-01	4 16 18.0	-55 23 29	19.23	0.30	14.6	17.1	23.8	4.3	7.2	25.6	
7731-01	4 17 13.0	-55 24 59	19.64	0.95	16.5	19.4	23.6	4.4	7.4	25.4	
7778-01	4 17 59.0	-55 24 44	18.95	0.46	24.2	25.5	23.1	4.9	8.1	25.0	
7783-01	4 18 56.9	-55 25 02	19.41	1.40	16.4	19.5	23.0	3.5	5.8	24.8	
7952-01	4 17 16.6	-55 25 03	19.53	1.60	14.9	17.2	23.4	3.7	6.1	25.3	
1064-03	4 15 50.1	-54 40 05	18.34	1.10	24.3	27.9	23.5	6.2	10.3	25.4	dE
88-05	4 13 15.9	-56 44 08	19.74	1.07	14.0	15.8	23.8	3.8	6.4	25.6	dE
1977-05	4 11 03.3	-56 24 27	19.13	0.82	14.7	16.2	23.2	3.1	5.2	25.0	dE
2674-06	4 10 35.3	-57 10 54	19.84	-0.23	15.4	17.5	23.1	3.3	5.5	25.0	dIrr ^(b)
1374-09	4 27 13.2	-55 38 52	18.67	0.85	18.4	21.9	22.8	3.8	6.3	24.7	dE
3330-10	4 03 04.9	-55 18 53	18.46	2.26	21.1	20.5	22.7	3.4	5.7	24.5	dIrr ^(c)
1116-11	4 23 41.1	-56 45 03	18.17	0.94	18.5	23.3	22.7	3.8	6.4	24.5	dIrr
1649-11	4 22 33.1	-56 41 09	19.00	1.15	19.3	21.3	24.2	6.4	10.7	26.0	dE
3041-11	4 22 52.9	-56 37 27	17.89	0.72	33.8	37.9	23.3	7.6	12.7	25.1	dIrr ^(b)
3854-d-02	4 15 17.0	-54 58 57	20.08	1.63	14.8 ^(e)	16.8 ^(e)	22.9	2.6	4.3	24.7	dIrr ^(b)
802-d-07	4 23 19.2	-55 46 45	18.85	1.00	15.6 ^(e)	17.0 ^(e)	22.5	2.3	3.9	24.4	dE

Table 3—Continued

ID	$\alpha(2000)$ [^h ^m ^s]	$\delta(2000)$ [[°] ['] ^{''}]	$V^{(a)}$ [mag]	$(V - I)^{(a)}$ [mag]	D_{26} [^{''}]	θ_{26} [^{''}]	$\mu_0(V)$ [mag/ ^{□''}]	h [^{''}]	r_{eff} [^{''}]	$\mu_{eff}(V)$ [mag/ ^{□''}]	Type
(1)	(2)	(3)	(4)	(5)	(6)	(7)	(8)	(9)	(10)	(11)	(12)
1961-d-07	4 21 05.3	-55 40 10	18.95	1.47	18.4 ^(e)	16.4 ^(e)	22.6	2.3	3.9	24.5	dE
2029-d-08	4 10 33.5	-55 30 15	19.57	0.80	14.7 ^(e)	15.5 ^(e)	24.6	3.8	6.4	26.4	dE
3714-d-10	4 02 07.8	-55 19 24	19.49	0.95	14.3 ^(e)	16.0 ^(e)	23.5	2.9	4.8	25.3	dE
L01 ^(f)	4 12 25.5	-56 05 31	18.50	...	29.2	30.4	24.8	13.3	22.2	26.6	dE
L02 ^(f)	4 14 56.2	-55 31 22	17.71	...	38.4	39.1	24.9	19.6	32.7	26.7	dE ^(d)
L03 ^(f)	4 14 37.4	-55 25 27	18.97	...	22.7	29.9	24.7	7.5	12.5	26.5	dE
L04 ^(f)	4 14 44.2	-55 24 54	19.12	...	23.2	25.7	24.9	12.9	21.5	26.7	dE

^(a)Not corrected according to the simulation in sec. 2.6 and not corrected by interstellar absorption.

^(b)Shows knots of star formation regions.

^(c)Red irregular galaxy.

^(d)Extended irregular low-surface brightness cloud located $\sim 10'$ to the NW of the NGC1549 galaxy.

^(e)Limiting isophotal diameter and diameter given by relation (4) at the surface brightness of 26.5 V mag/arcsec².

^(f)These galaxies were not detected in the I filter (see section 2.7).

Table 4. Completeness fraction for point sources

Magnitude (bin) (1)	$f(V)^{(a)}$ [CTIO] (2)	$\sigma_{f(V)}^{(b)}$ [CTIO] (3)	$f(V)^{(a)}$ [LCO] (4)	$\sigma_{f(V)}^{(b)}$ [LCO] (5)
16.0 - 16.5	0.99	0.04	1.00	0.01
16.5 - 17.0	0.98	0.04	1.00	0.01
17.0 - 17.5	0.98	0.03	1.00	0.01
17.5 - 18.0	0.96	0.03	1.00	0.01
18.0 - 18.5	0.96	0.05	1.00	0.01
18.5 - 19.0	0.96	0.05	1.00	0.01
19.0 - 19.5	0.93	0.05	0.99	0.03
19.5 - 20.0	0.91	0.06	0.99	0.03
20.0 - 20.5	0.88	0.07	0.99	0.04
20.5 - 21.0	0.45	0.13	0.97	0.04
21.0 - 21.5	0.97	0.03
21.5 - 22.0	0.95	0.04
22.0 - 22.5	0.92	0.06
22.5 - 23.0	0.92	0.06
23.0 - 23.5	0.89	0.08
23.5 - 24.0	0.66	0.10

^(a) $f(V)$: detected fraction in the V band

^(b) $\sigma_{f(V)}$: one standard deviation in $f(V)$

Table 5. Average completeness fraction for LSB disk galaxies

Magnitude (bin)	$f(V)^{(a)}$ [CTIO]	$\sigma_{f(V)}^{(b)}$ [CTIO]	$f(V)^{(a)}$ [LCO]	$\sigma_{f(V)}^{(b)}$ [LCO]
(1)	(2)	(3)	(4)	(5)
16.0 - 16.5	0.77	0.04	0.75	0.08
16.5 - 17.0	0.83	0.01	0.83	0.04
17.0 - 17.5	0.83	0.01	0.82	0.09
17.5 - 18.0	0.84	0.06	0.85	0.07
18.0 - 18.5	0.82	0.07	0.91	0.07
18.5 - 19.0	0.71	0.06	0.86	0.04
19.0 - 19.5	0.73	0.06	0.87	0.03
19.5 - 20.0	0.53	0.10	0.84	0.06
20.0 - 20.5	0.78	0.07
20.5 - 21.0	0.60	0.27

^(a) $f(V)$: detected fraction in the V band

^(b) $\sigma_{f(V)}$: one standard deviation in $f(V)$

Table 6. Monte Carlo simulations: photometric and scale length errors

Session (1)	CSB interval ^(a) (2)	V_{inp} (3)	$\Delta(V)$ ^(b) (4)	$\sigma_{\Delta(V)}$ ^(c) (5)	$\Delta(\mu_0)$ ^(d) (6)	$\sigma_{\Delta(\mu_0)}$ ^(e) (7)	$\Delta h/h$ ^(f) (8)	$\sigma_{\Delta h/h}$ ^(g) (9)
CTIO	22.5 - 23.5	16.25	-0.08	0.05	0.09	0.09	-0.06	0.06
		16.75	-0.07	0.06	0.05	0.10	-0.08	0.06
		17.25	-0.07	0.08	-0.02	0.11	-0.13	0.08
		17.75	-0.07	0.07	-0.08	0.13	-0.18	0.09
	23.5 - 24.5	16.25	-0.17	0.09	0.20	0.09	-0.01	0.07
		16.75	-0.18	0.08	0.18	0.11	-0.02	0.08
		17.25	-0.14	0.10	0.15	0.13	-0.04	0.09
		17.75	-0.13	0.12	0.11	0.14	-0.10	0.15
		18.25	-0.13	0.11	0.07	0.18	-0.10	0.14
	24.5 - 25.5 ^(h)	18.75	-0.13	0.13	0.02	0.19	-0.16	0.17
		17.75	-0.27	0.23	-0.56	0.11	-0.20	0.25
		18.25	-0.29	0.20	-0.93	0.16	-0.20	0.11
		18.75	-0.24	0.21	-1.23	0.13	-0.35	0.33
		19.25	-0.24	0.19	-1.49	0.17	-0.40	0.31
		19.75	0.10	0.51	-1.64	0.21	-0.43	0.41
LCO40	22.5 - 23.5	16.25	-0.09	0.05	0.08	0.08	-0.03	0.03
		16.75	-0.07	0.04	0.04	0.09	-0.05	0.04
		17.25	-0.06	0.04	0.03	0.09	-0.06	0.04
		17.75	-0.04	0.05	0.02	0.09	-0.07	0.05
		18.25	-0.05	0.05	-0.02	0.09	-0.09	0.05
		18.75	-0.04	0.05	-0.05	0.11	-0.12	0.06
	23.5 - 24.5	16.25	-0.13	0.11	0.14	0.09	0.02	0.05
		16.75	-0.11	0.09	0.13	0.09	-0.01	0.05
		17.25	-0.15	0.08	0.13	0.10	-0.03	0.06
		17.75	-0.13	0.08	0.13	0.10	-0.05	0.06
		18.25	-0.10	0.08	0.09	0.08	-0.07	0.06
		18.75	-0.09	0.06	0.10	0.10	-0.08	0.08
	24.5 - 25.5	19.25	-0.07	0.09	0.04	0.11	-0.10	0.09
		19.75	-0.08	0.09	0.01	0.13	-0.14	0.08
		16.75	-0.27	0.18	0.26	0.11	0.16	0.11
		17.25	-0.21	0.17	0.29	0.10	0.10	0.10
		17.75	-0.22	0.18	0.27	0.11	0.07	0.11

Table 6—Continued

Session (1)	CSB interval ^(a) (2)	V_{inp} (3)	$\Delta(V)$ ^(b) (4)	$\sigma_{\Delta(V)}$ (5)	$\Delta(\mu_0)$ ^(d) (6)	$\sigma_{\Delta(\mu_0)}$ ^(e) (7)	$\Delta h/h$ ^(f) (8)	$\sigma_{\Delta h/h}$ ^(g) (9)
		18.25	-0.18	0.19	0.27	0.11	0.05	0.10
		18.75	-0.21	0.15	0.28	0.12	0.01	0.10
		19.25	-0.19	0.16	0.27	0.12	0.00	0.10
		19.75	-0.18	0.16	0.19	0.14	-0.02	0.10
		20.25	-0.14	0.16	0.14	0.16	-0.14	0.14
		20.75	-0.01	0.17	0.11	0.22	-0.34	0.14
	25.5 - 26.5 ^(h)	17.75	-0.29	0.24	-0.22	0.10	0.03	0.15
		18.25	-0.16	0.20	-0.19	0.14	0.03	0.13
		18.75	-0.15	0.19	-0.26	0.12	-0.06	0.16
		19.25	-0.12	0.14	-0.36	0.12	-0.07	0.12
		19.75	-0.16	0.18	-0.33	0.15	-0.12	0.21
		20.25	-0.12	0.15	-0.47	0.14	-0.34	0.37
		20.75	-0.33	0.41	-0.61	0.20	-0.25	0.14

^(a)Central surface brightness interval (mag/arcsec²).

^(b) $\Delta(V) = V_{inp} - V_{out}$: difference bewteen input and output magnitudes.

^(c) $\sigma_{\Delta(V)}$: one standard deviation in $\Delta(V)$.

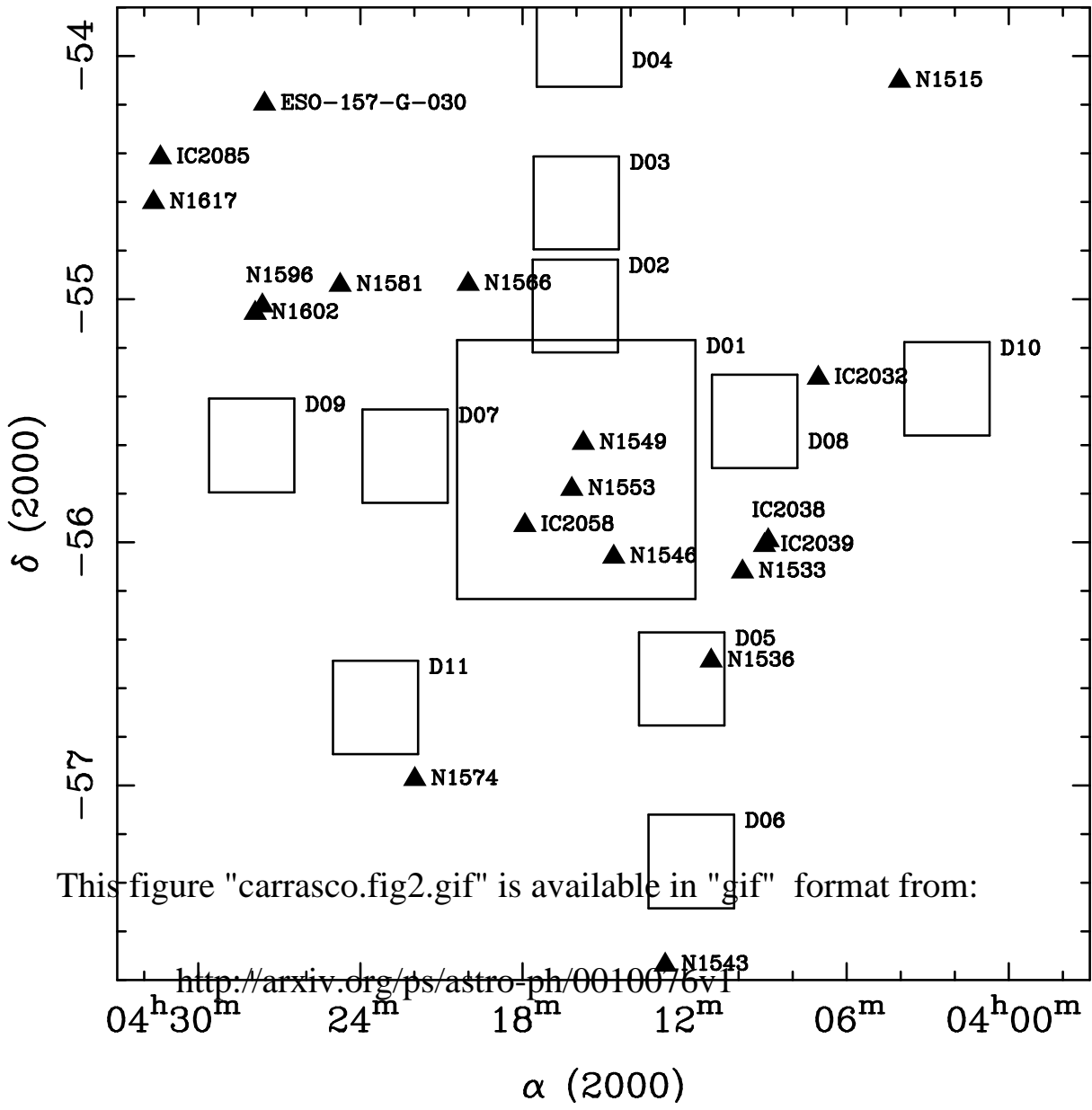
^(d) $\Delta(\mu_0) = \mu_0^{inp} - \mu_0^{out}$: differences between input and output central surface brightnesses (mag/arcsec²).

^(e) $\sigma_{\Delta(\mu_0)}$: one standard deviation in $\Delta(\mu_0)$ (mag/arcsec²).

^(f) $\Delta h/h = (h_{inp} - h_{out})/h_{inp}$: differences between input and output scale length in percentage.

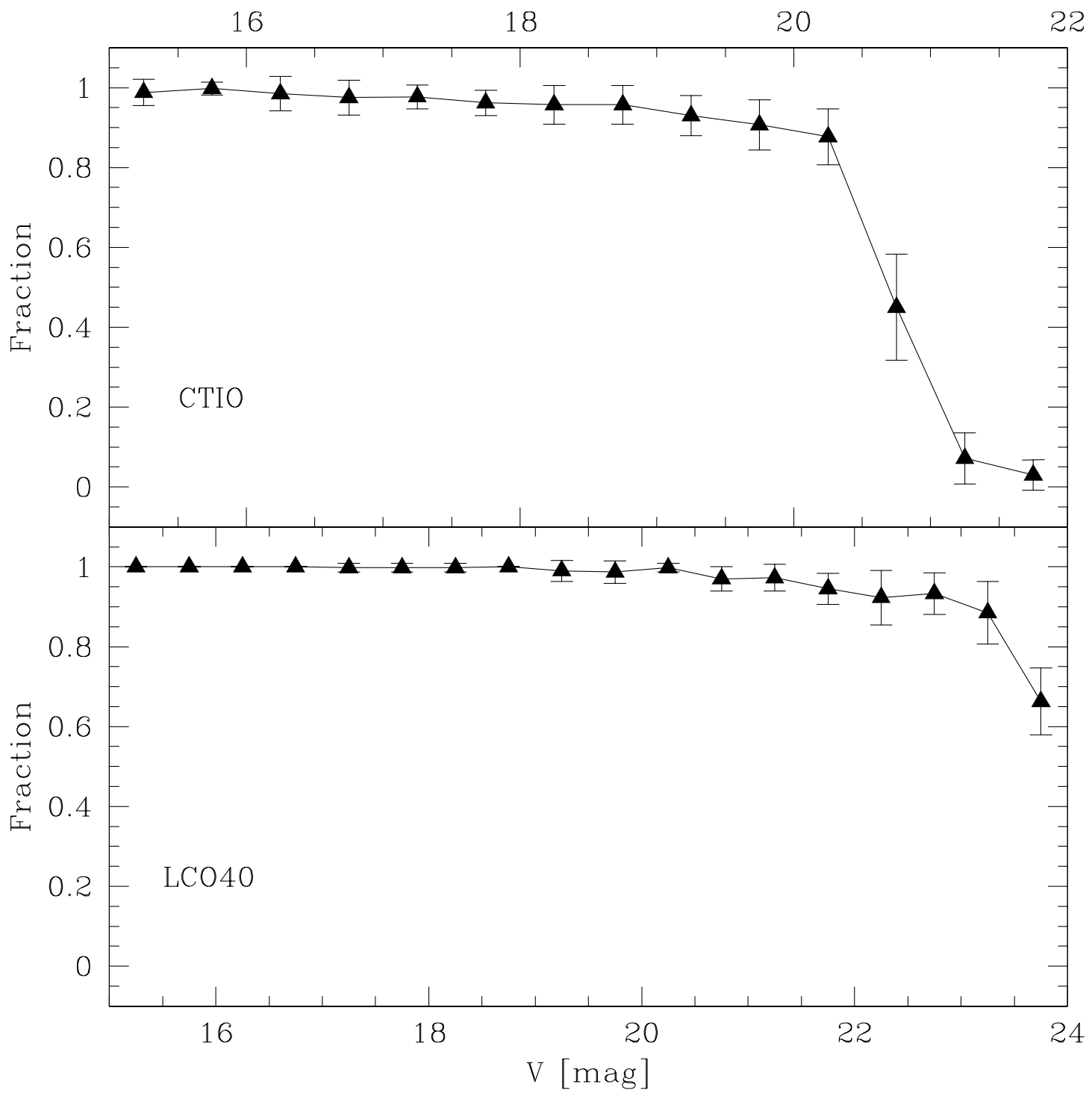
^(g) $\sigma_{\Delta h/h}$: one standard deviation in $\Delta h/h$.

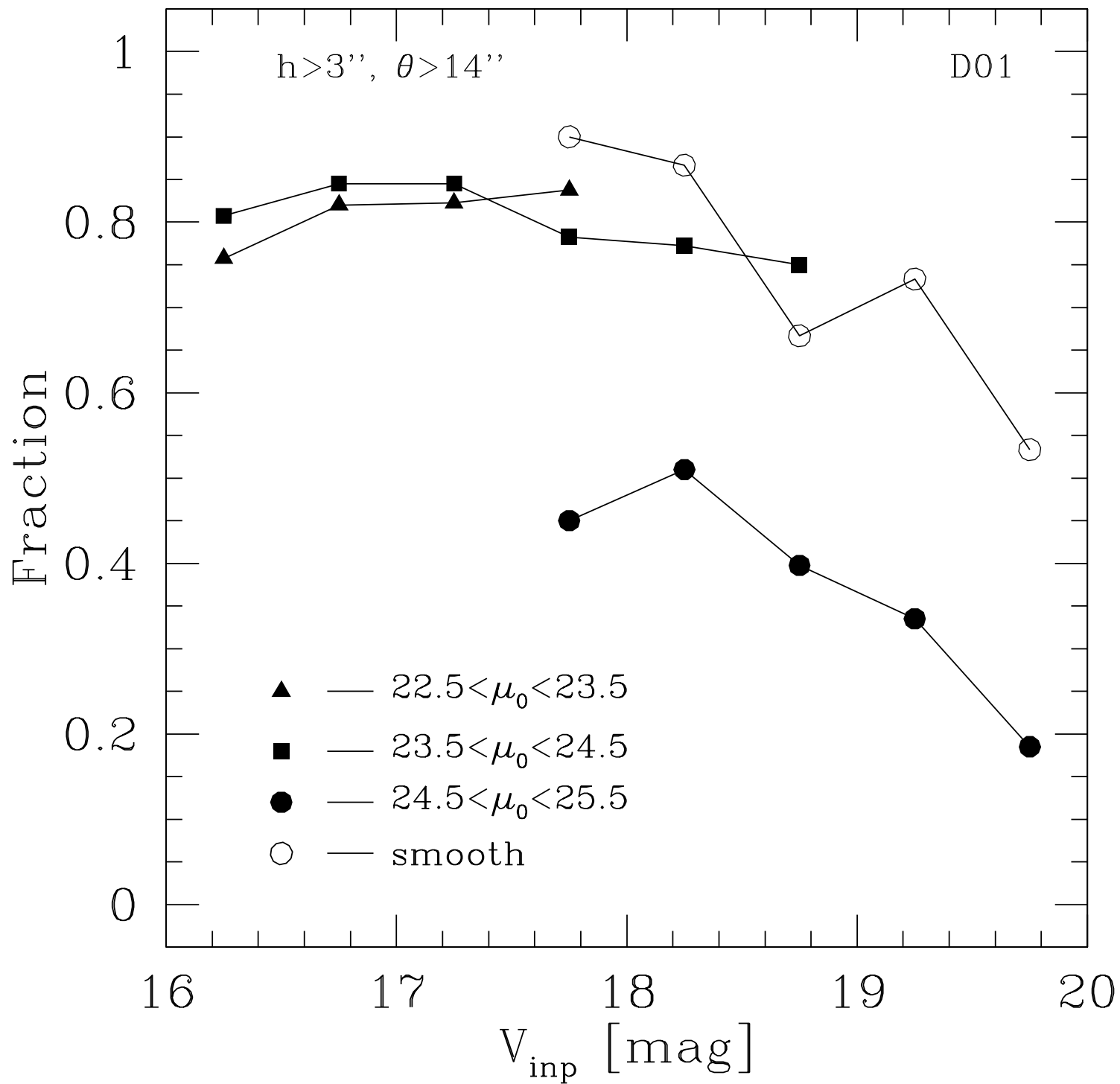
^(h)The results showed in the last bins of surface brightnesses for the CTIO and LCO40 data were obtained using the smoothing method described in section 2.7.

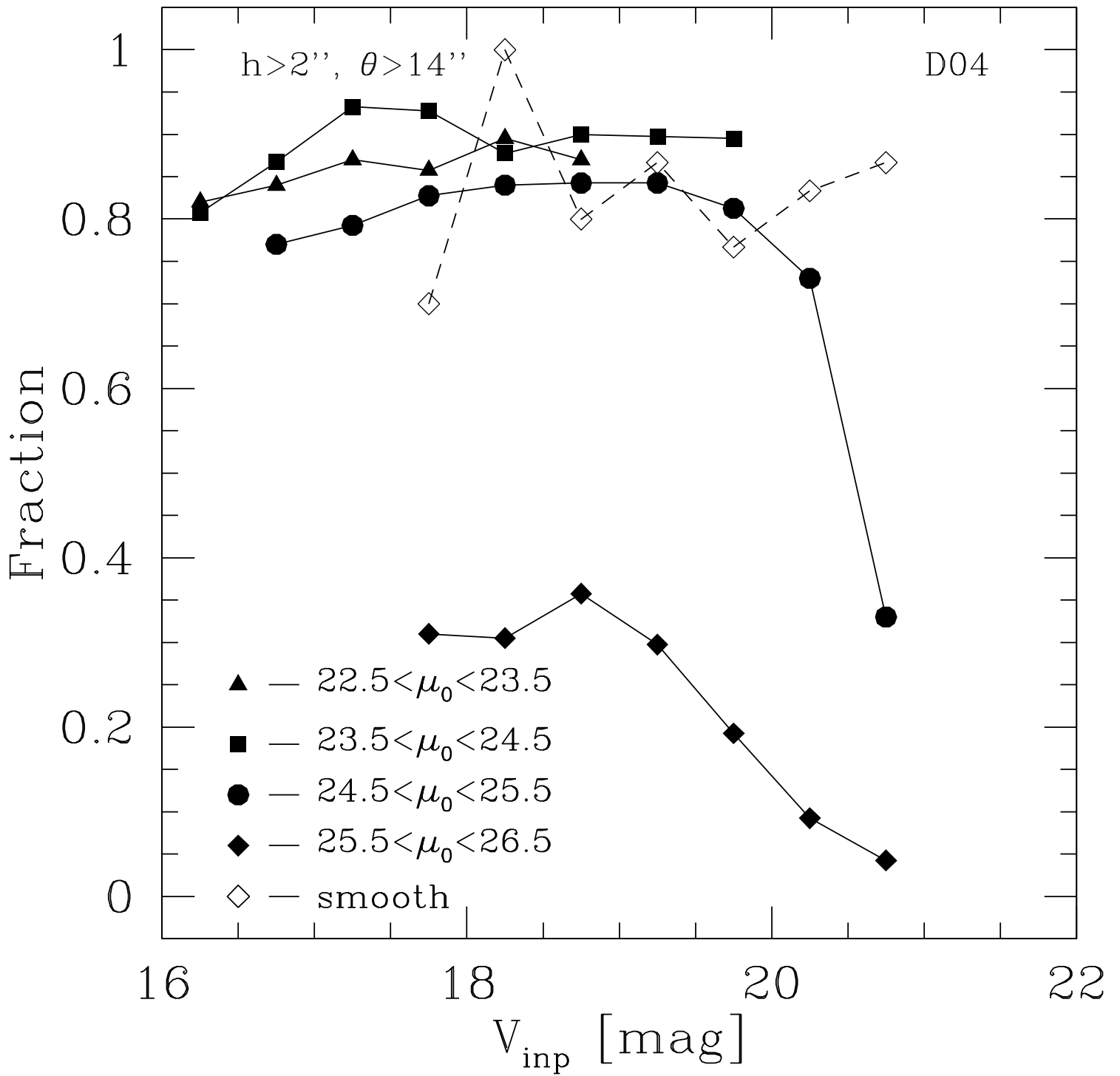


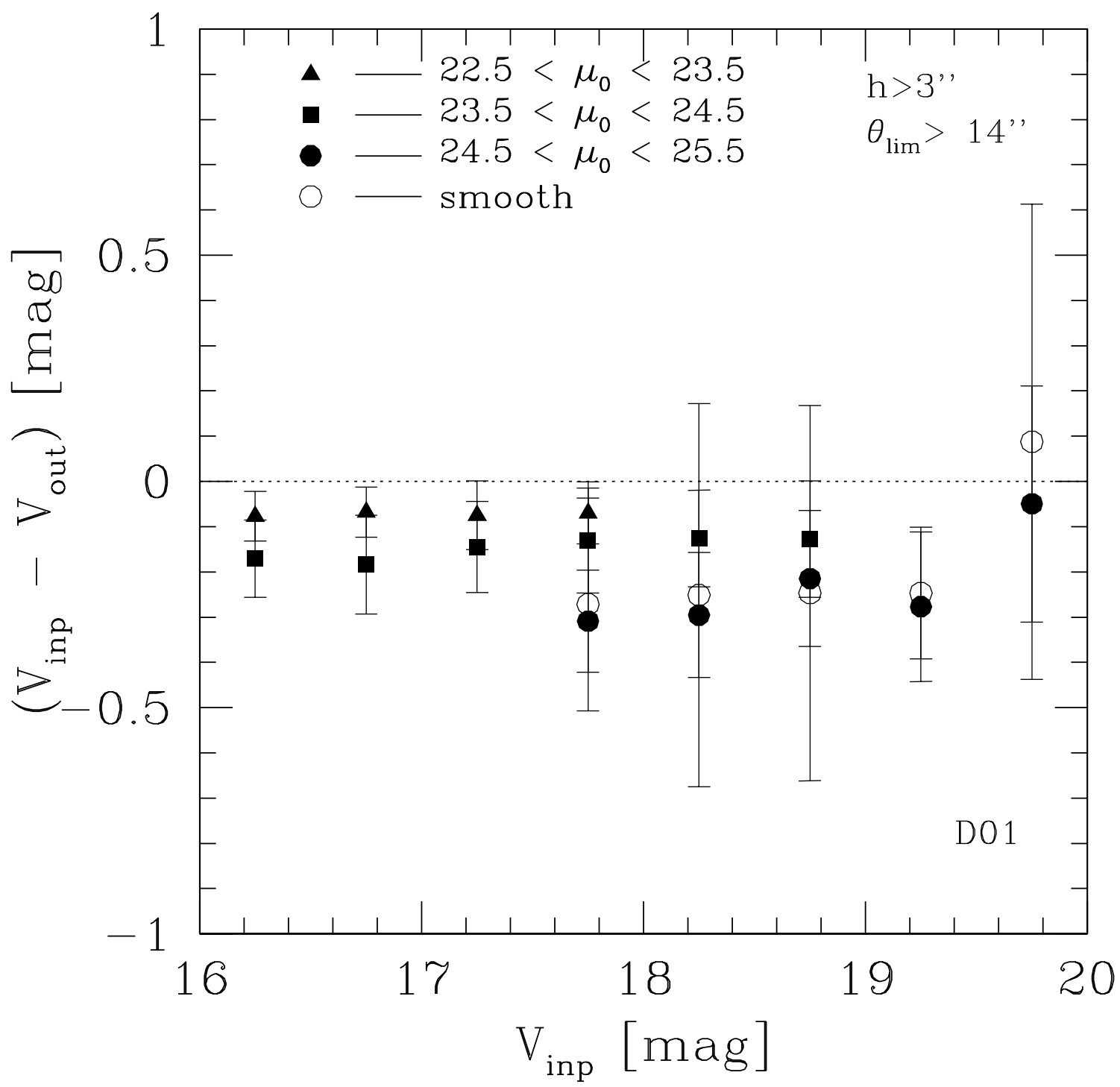
This figure "carrasco.fig2.gif" is available in "gif" format from:

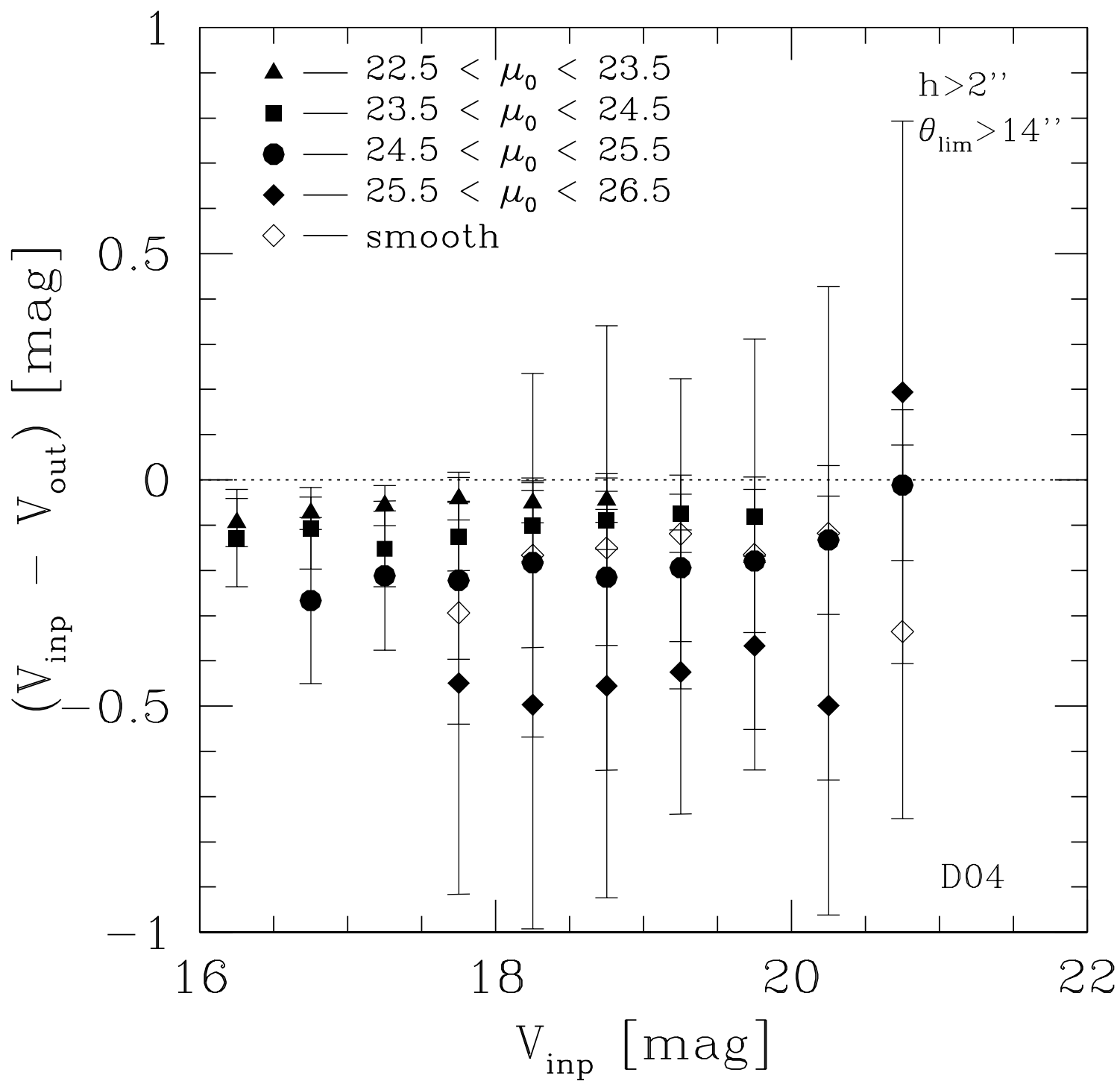
<http://arxiv.org/ps/astro-ph/0010076v1>









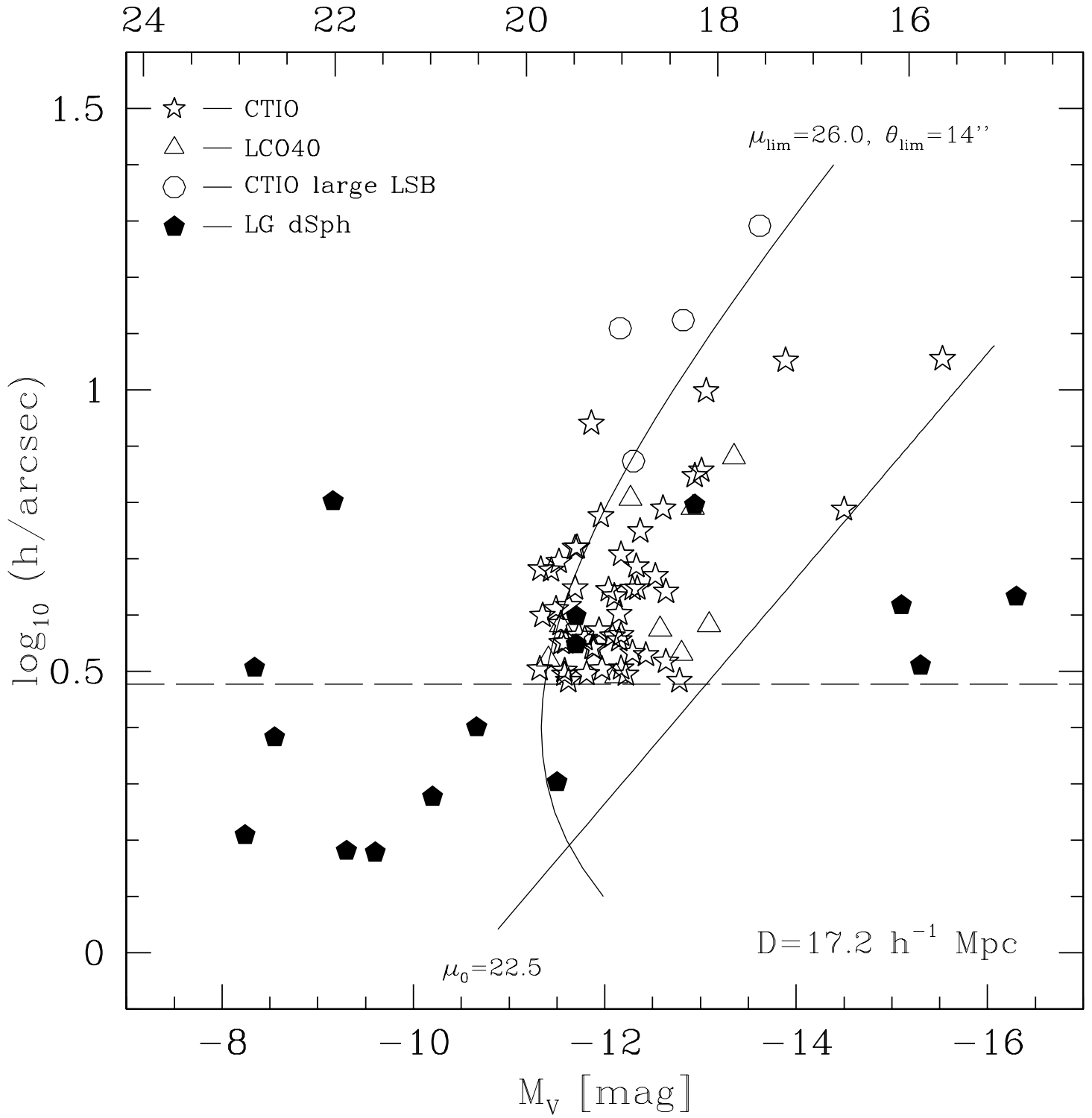


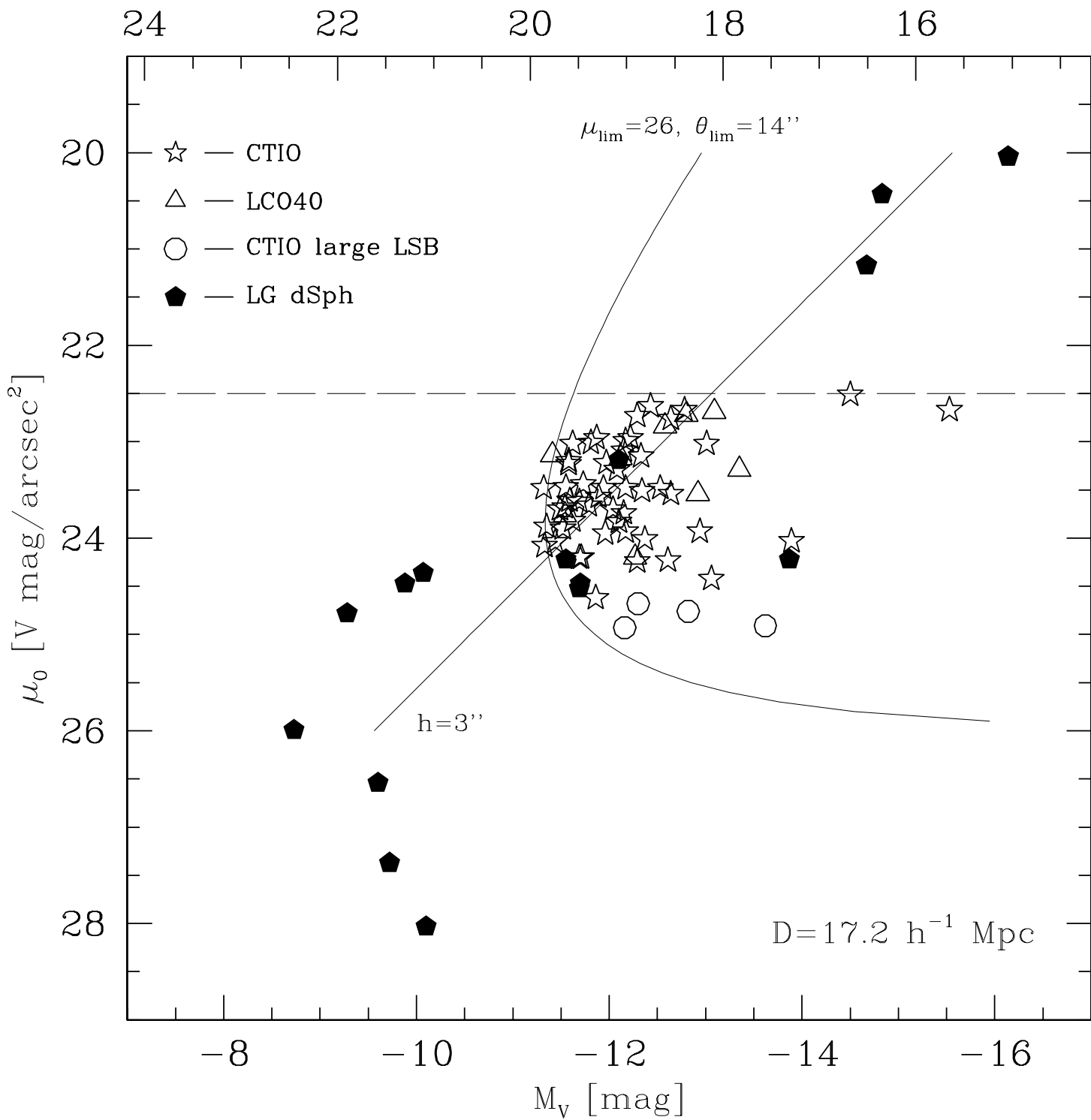
This figure "carrasco.fig6.gif" is available in "gif" format from:

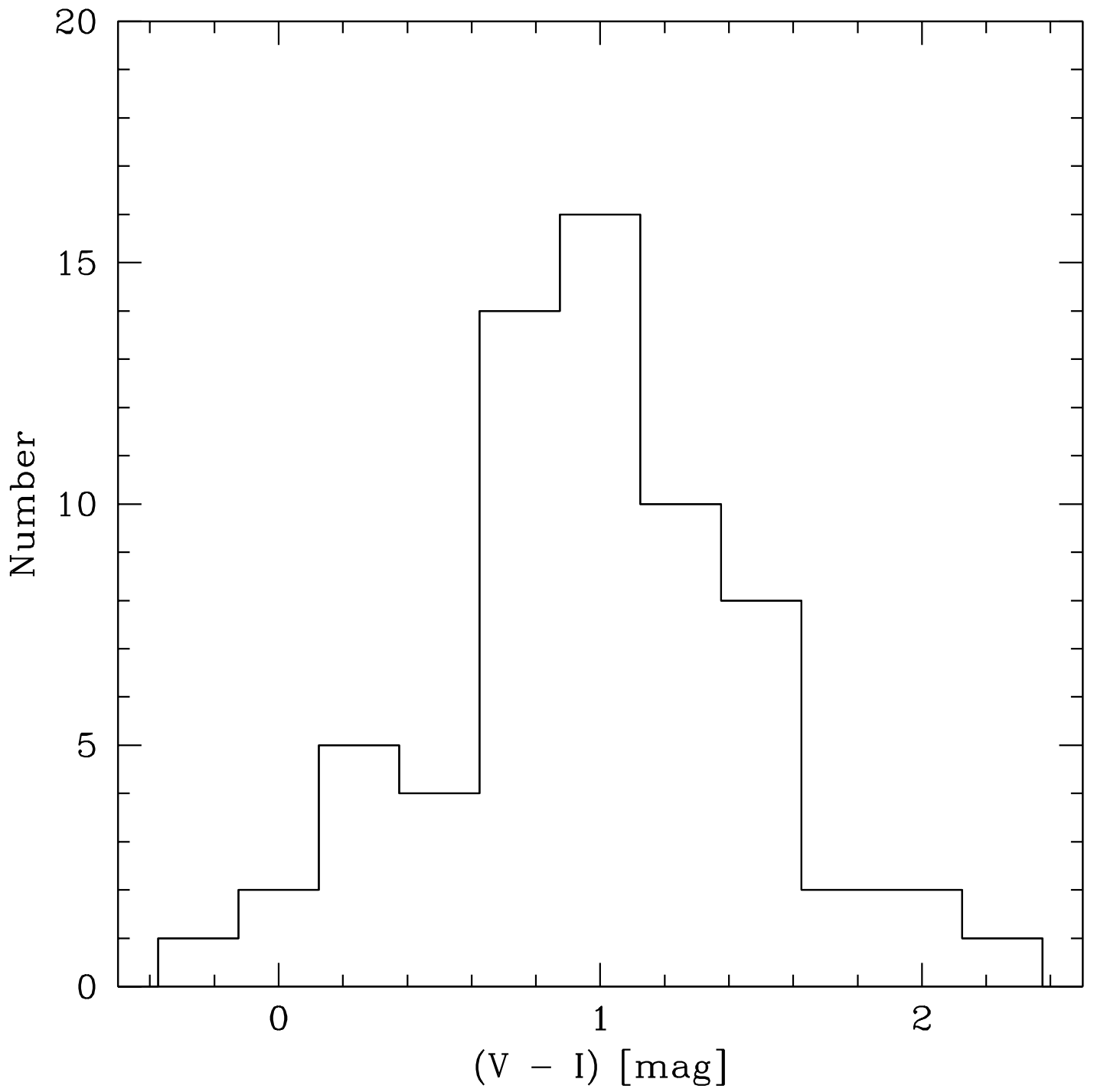
<http://arxiv.org/ps/astro-ph/0010076v1>

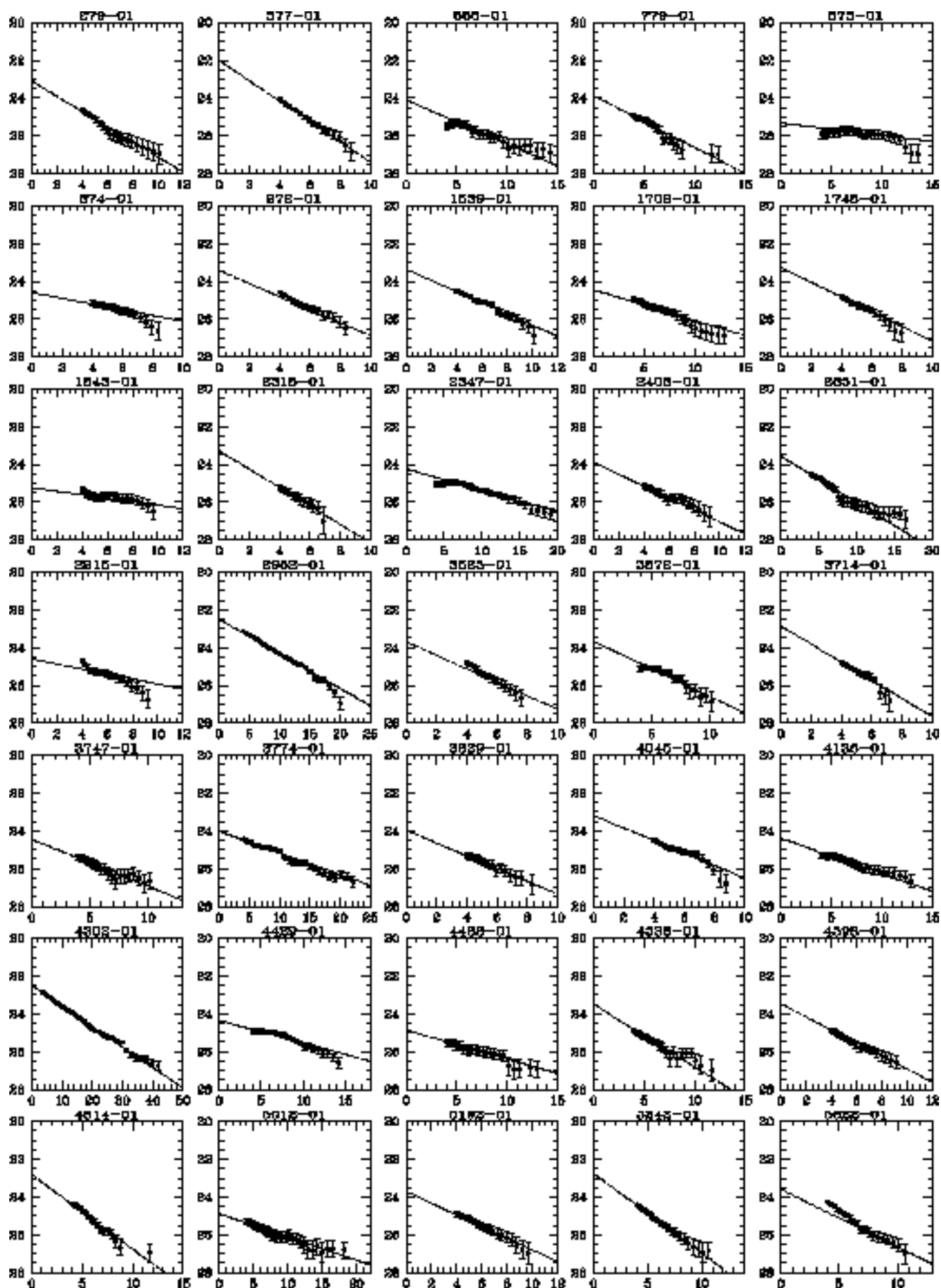
This figure "carrasco.fig7.gif" is available in "gif" format from:

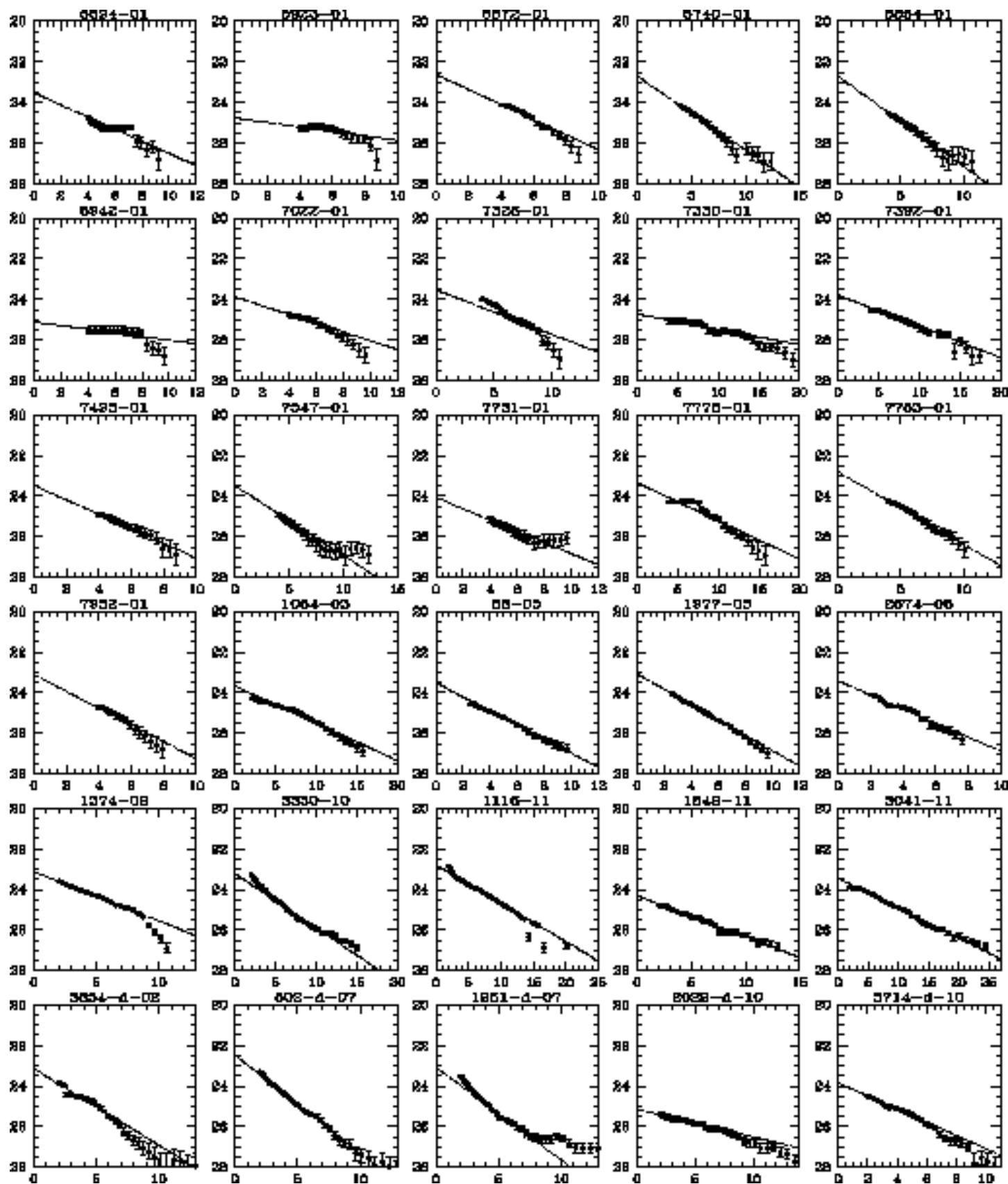
<http://arxiv.org/ps/astro-ph/0010076v1>

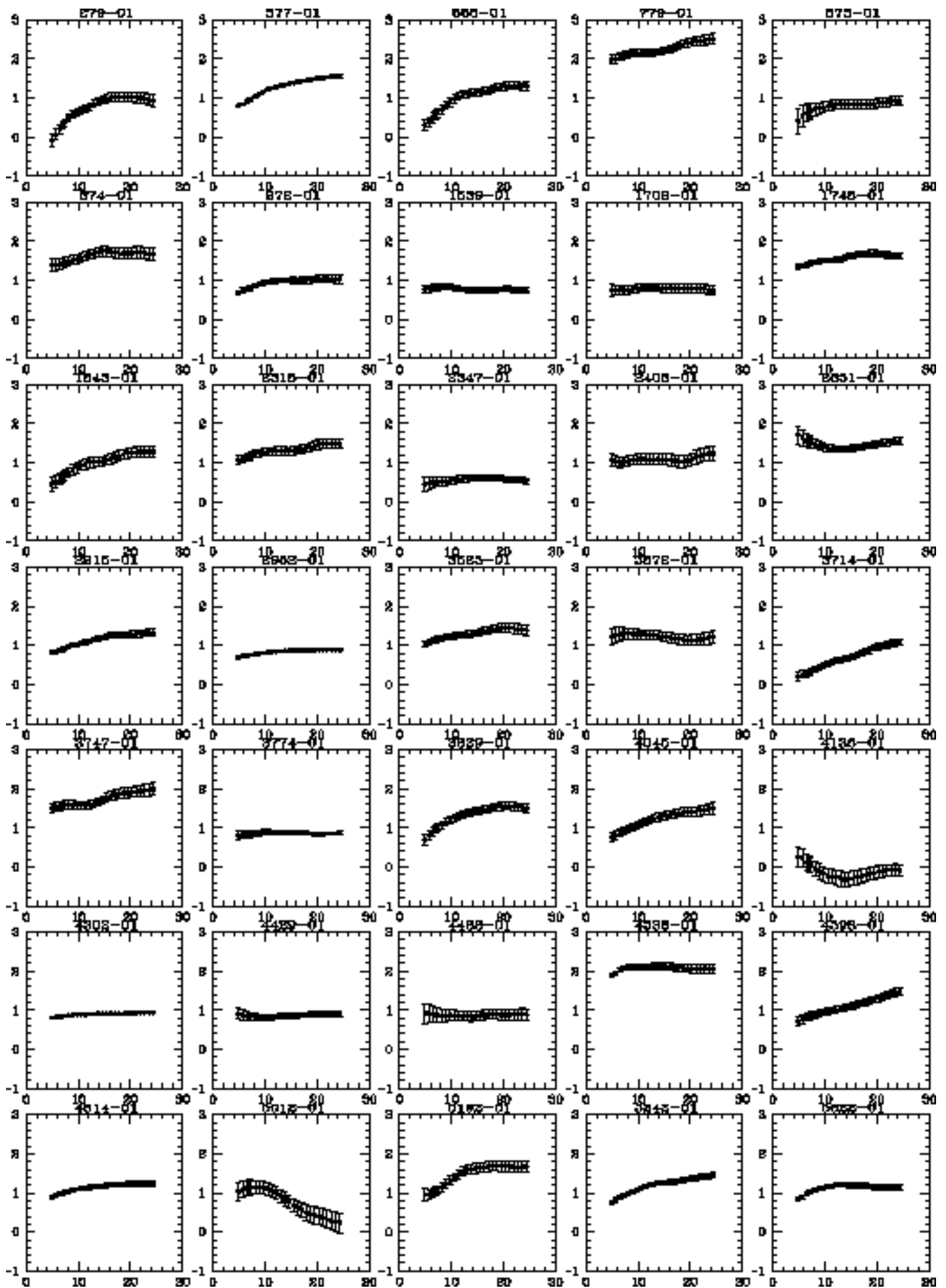


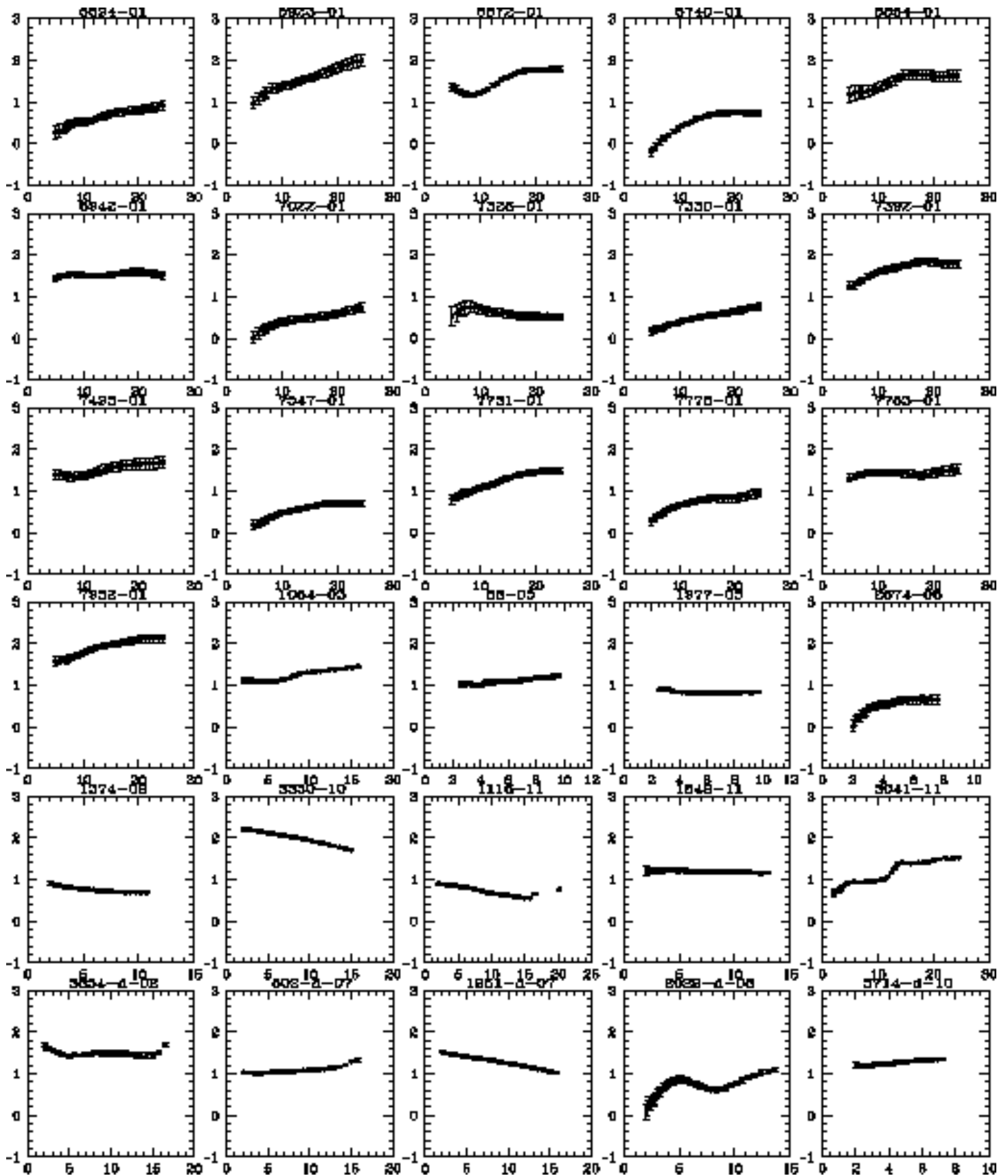


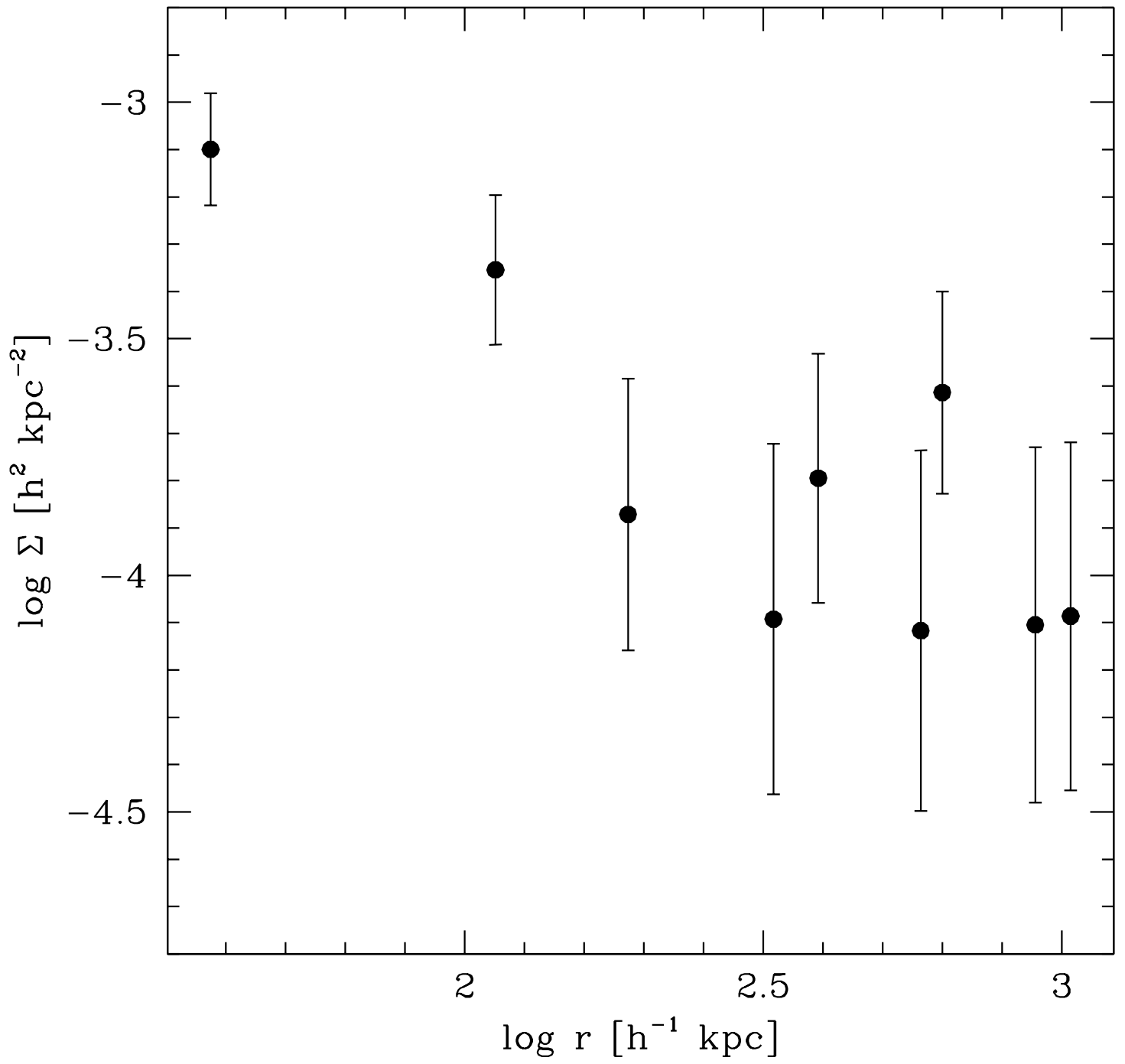












54

